

METHODS AND APPLICATIONS OF HYDROGEN PEROXIDE ANALYSIS
IN FRESHWATER SYSTEMS

by

Taylor C. Dixon

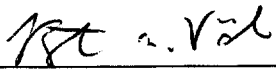
A thesis submitted to the faculty and the Board of Trustees of the Colorado School of Mines in partial fulfillment of the requirements for the degree of Master of Science (Hydrology).

Golden, Colorado

Date 4/13/10

Signed: 


Taylor C. Dixon

Signed: 

Dr. Bettina M. Voelker
Thesis Advisor

Golden, Colorado

Date 4/13/2010

Signed: 

Dr. John E. McCray
Professor and Director
Hydrologic Science and Engineering Program

Signed: 

Dr. Daniel M. Knauss
Professor and Head
Department of Chemistry and Geochemistry

ABSTRACT

Hydrogen peroxide (H_2O_2) is known to play key roles in aquatic systems, including metal redox cycling and degradation of organic matter into bioavailable forms. Additionally, H_2O_2 has been observed to affect the growth and health of aquatic biological communities. Detailed knowledge of the cycling of H_2O_2 in natural waters thus fosters the understanding of important aquatic biogeochemical processes.

In Chapter 1, the analytical method used to measure H_2O_2 in freshwater systems is described in detail, including specific modifications to the well-known method to allow for accurate quantification of *in situ* H_2O_2 concentrations. Critical information regarding reagent stability and precautionary measures to be taken when applying the method to freshwater systems are also presented.

In the experiments described in Chapter 2, the H_2O_2 method and an additional method used to measure an isotopically-labeled H_2O_2 tracer were applied to a freshwater stream in eastern Nebraska. The specific goal was to characterize the importance of absolute rates of *in situ* microbiological production of H_2O_2 to the freshwater system studied. Although biological production of H_2O_2 has been observed in culture studies, the significance of this process to the H_2O_2 budget in freshwater systems had not previously been investigated. In this study, isotopically-labeled H_2O_2 ($\text{H}_2^{18}\text{O}_2$) was added to novel in-stream mesocosm systems exposed to light and dark periods. By measuring total H_2O_2 and $\text{H}_2^{18}\text{O}_2$ in tandem, we inferred absolute rates of H_2O_2 production and decay, which were occurring simultaneously. This investigation is the first to characterize absolute rates of freshwater H_2O_2 production *in situ*, and suggests biological production as the dominant control on the H_2O_2 budget in the agricultural headwater stream studied. Further, the results indicate rates of H_2O_2 production up to several-fold the photo-

production rates observed in filtered water samples, supporting the need for *in situ* measurements to understand surface water H₂O₂ cycling.

TABLE OF CONTENTS

ABSTRACT	iii
LIST OF FIGURES	vii
LIST OF TABLES	ix
ACKNOWLEDGEMENTS	x
CHAPTER 1 TOTAL HYDROGEN PEROXIDE ANALYSIS METHOD	1
1.1 Equipment	1
1.2 Materials	2
1.3 Method Setup	3
1.4 Chemiluminescence Mechanism	4
1.5 Reagent Stability	5
1.6 Method Calibration and Chelator Use.....	7
1.7 Method Precautions for Freshwater Systems	10
CHAPTER 2 HYDROGEN PEROXIDE DYNAMICS IN AN AGRICULTURAL HEADWATER STREAM: EVIDENCE FOR SIGNIFICANT BIOLOGICAL PRODUCTION	12
2.1 Introduction	12
2.2 Methods	17
2.2.1 H ₂ ¹⁸ O ₂ Method	17
2.2.2 Materials for H ₂ ¹⁸ O ₂ Method.....	18
2.2.3 Site Location	18
2.2.4 Experimental Setup	19
2.2.5 Sampling and Method Calibration	22
2.3 Modeling	24
2.3.1 Modeling the Decay	25
2.3.2 Modeling the Dark Production	26
2.3.3 Modeling the Light Production	27
2.4 Results	29
2.4.1 Input Concentrations and Flushing Coefficients.....	29
2.4.2 Measured Concentrations	30
2.4.3 Decay Coefficients	31
2.4.4 Overview of Production Processes	34
2.4.5 Modeling the Dark Production	34

2.4.6	Modeling the Light Production	37
2.5	Discussion	40
2.5.1	Rates of Decay	40
2.5.2	Production Processes	43
2.6	Conclusions	46
	REFERENCES CITED	48
	APPENDIX	53

LIST OF FIGURES

Figures 1.1a and b	Schematic of the FIA system illustrating the sample filling the sample loop (a) and the injection valve switching to inject the sample into the flow cell for analysis (b), courtesy of Waterville Analytical.....	4
Figure 1.2	Chemiluminescence-generating reaction mechanism exploited in the AE-CL method (Cooper et al. 2000).....	5
Figure 1.3	Standard additions calibration in a sample matrix of 0.2 μm filtered stream water.....	7
Figure 1.4	Effects of the addition of 5 μM Fe(II), 10 μM Mn(II), 100 μM Ferrozine, and 100 μM DTPA on AE-CL measured $[\text{H}_2\text{O}_2]$	10
Figure 2.1	Depiction of in-stream opened-bottom mesocosm setup (i.e. M1 and M2). Arrows indicate direction of water flow (i.e. down through sediment). Closed-bottom controls (i.e. MC) were setup in a similar fashion, but with the addition of an outlet line opposite to the circulation pump. Also, closed-bottom controls were not forced into the stream sediment.....	21
Figures 2.2a – d	Measured $[\text{H}_2\text{O}_2]$ (a and b) and $[\text{H}_2^{18}\text{O}_2]$ (c and d) during days 1 and 2. The early morning time periods were also in the dark.....	31
Figure 2.3	Modeled absolute decay constants (k_d) in each mesocosm. Error bars represent the k_d values associated with the 90% confidence interval upper and lower $[\text{H}_2^{18}\text{O}_2]$ listed in Table 2.1.....	33
Figure 2.4	Comparison of measured and modeled $[\text{H}_2\text{O}_2]$ without P_{dark} , assuming constant P_{dark} , and changing P_{dark} according to (2.5) and (2.7).....	36
Figure 2.5	Modeled P_{dark} for each mesocosm according to (2.5) and (2.7). The uncertainty is depicted by the solid and dashed lines for the opened- and closed-bottom mesocosms, respectively. The high limit of uncertainty for M1 and M2 is not shown for scale clarity.....	36
Figures 2.6a and b	Comparison of measured and modeled $[\text{H}_2\text{O}_2]$ during the light period using the non-linear- P_{light} model (days 1 and 2 presented in a and b, respectively).....	38

Figure 2.7	Modeled P_{light} for each mesocosm according to (2.9) and (2.11). The uncertainty is depicted by the solid and dashed lines for the opened- and closed-bottom mesocosms, respectively. The high limit of uncertainty for M1 and M2 is not shown.....	38
Figures 2.8a and b	Bar graphs of initial and final P_{light} and P_{dark} for the opened- and closed-bottom mesocosms during day 2 (presented in a and b, respectively). The average production rates of M1 and M2 were used to calculate production rates in Figure 2.8a. The hatched boxes represent the contributions of abiotic photo- production (P_{photo}).....	46

LIST OF TABLES

Table 2.1	First-order k_f and associated T_r for each mesocosm. T_r was calculated according to (1), and k_f was calculated as the inverse of T_r	30
Table 2.2	Steady-state $[H_2^{18}O_2]$ associated with the overall best-fit k_d value and 90% confidence interval $[H_2^{18}O_2]$ used to calculate uncertainty in k_d (i.e. low $[H_2^{18}O_2]$ used to obtain high k_d , and vice versa). All concentrations listed are in nM.....	32
Table 2.3	Agreement of $P_{bio,light}$ and P_{dark} during day 2 at the time of transition between light and dark periods (i.e. 15:00) when $P_{bio,light}$ is modeled as the difference between P_{light} and $P_{photo} = 0.5 \mu M h^{-1}$	39

ACKNOWLEDGEMENTS

Over the last two years, several organizations and people have contributed notably to my success at Colorado School of Mines. The Hydrologic Science and Engineering (HSE) Program, the academic organization that laid the foundation for my M.S. degree, proved to be top-notch, in terms of unparalleled professors, coursework applicability to real world challenges, and the flexibility enabling me to intertwine my ambitions in physical hydrology and environmental chemistry. Equally impressive is the Department of Chemistry and Geochemistry, which ensured my funding sources were directed towards my research activities and my personal finances. Specifically, the administrative staff in the Department, through unyielding professionalism and reliability, guaranteed my graduate student experience was comfortable and enjoyable. I also thank my funding sources, the National Science Foundation, the American Water Works Association LARS Fellowship, and the HSE Program.

In thanking the countless number of people that have impacted my graduate studies, I would like to begin with Dr. Bettina Voelker. I first contacted Dr. Voelker during the summer of 2007, when I was feverishly researching prospective graduate programs. Of all the professors I contacted, at schools across the western U.S., Dr. Voelker was by far the most welcoming. Not only did she take the time to speak with me on numerous occasions, but she also expressed sincere interest in my wife's and my overall well being in the Denver area. My professional and personal relationship with Dr. Voelker only grew from there. Without her unmatched knowledge of our research arena, and the example she sets for balancing work and life, I would not have achieved my graduate degree in the same timeframe or with the same depth and confidence that I feel I attained.

I am also incredibly indebted to my previous colleague Dr. Andrew Vermilyea, now serving his post-doctoral research studies at the University of Alaska. Dr. Vermilyea shouldered the responsibility of training me in all hands-on aspects of conducting graduate level research.

His thorough understanding of the analytical techniques we employed, all relevant scientific fundamentals, and the technical details associated with conducting field-based research largely contributed to the success of my research activities. Not only did Dr. Vermilyea help me collect the data I needed to write my thesis, but he also provided me with the opportunity to co-author a journal publication. Further, his superhuman energy and hilarious demeanor made conducting numerous, grueling days of field experiments almost pleasant.

Other people that were instrumental in the success of my research activities were my committee members, Dr. Jim Ranville and Dr. John McCray, as well as Dr. Durelle Scott of Virginia Polytechnic and State University and Robert Reed of the Department of Chemistry and Geochemistry. Dr. Ranville and Dr. McCray provided critical insight to my thesis, and helped me shape the presentation of my findings in an applicable and understandable manner. Dr. Scott is the co-investigator of my project in Nebraska, and his knowledge in technical field work details guided my understanding of conducting hydrochemical field experiments. Robert Reed supplied his raw manpower to the field campaigns in 2009, without which I would not have been able to collect the data that ultimately formed the backbone of my thesis. Of course, his passion for cutoff jeans and Menards was also vital to our success in the field.

Additionally, I owe many graduate students at Colorado School of Mines heartfelt gratitude for their positive attitudes at school and at various off-campus events. In addition to being respectable scholars, the graduate students at Mines know how to dust off the stress and soak in the good times.

Finally, without the love and support of my beautiful wife, which guided me through the ups and downs of graduate school, I would not be where I am today. Her incredible smile has been, and always will be, what fuels my motivations and ambitions in life. Thank you, Afton.

CHAPTER 1

TOTAL HYDROGEN PEROXIDE ANALYSIS METHOD

The method of analysis for total hydrogen peroxide concentrations ($[H_2O_2]$) is based on the chemiluminescence generating reaction between 10-methyl-9-(p-formylphenyl) acridinium carboxylate trifluoromethanesulfonate (AE) and the conjugate base of H_2O_2 (HO_2^-). The method was pioneered by Cooper et al. (2000), and optimized by King et al. (2007) for use in flow injection analysis (FIA) systems. The method, hereafter referred to as the AE-CL method, has been utilized in the Voelker laboratory for several years. Following minor modifications to the procedures of King and Cooper, the AE-CL method has proven to be a convenient and consistent method of analysis for H_2O_2 . Further, this method yields measured $[H_2O_2]$ that are in good agreement with other H_2O_2 analysis methods (Cooper et al. 2000, Miller et al. 2005), and has the advantage of selectivity for H_2O_2 over other (organic) peroxides (Miller et al. 2005, King et al. 2007).

1.1 Equipment

The FIA system was developed by Waterville Analytical and consists of a Rainin Dynamax peristaltic pump in-line with a 10-port injection valve and Hamamatsu Corporation photomultiplier tube (PMT). Tygon tubing (1.02 mm ID) is used in conjunction with the peristaltic pump. All other system tubing is PEEK material (0.76 mm ID x 1.59 mm OD), and all connections are composed of polypropylene. The PMT signal is processed by FeLume(II) software (Waterville Analytical) installed on a laptop PC.

1.2 Materials

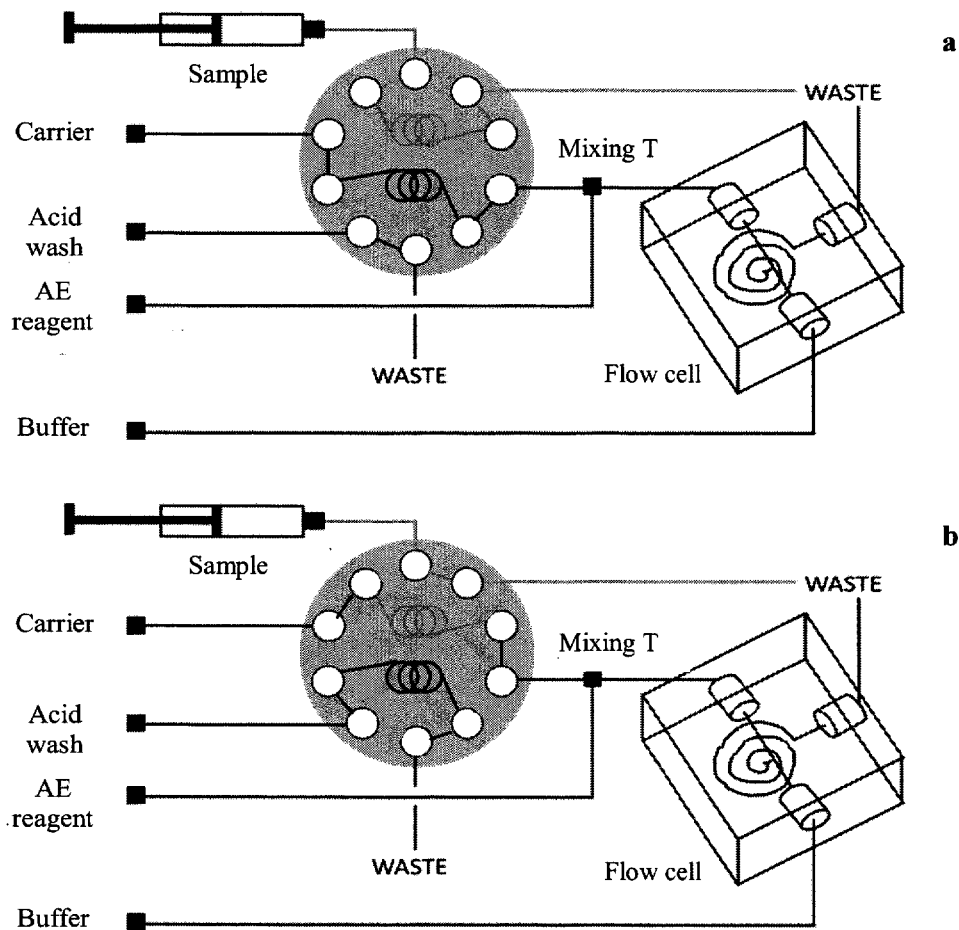
All reagent solutions are prepared in water purified with a NANOpure® Diamond™ UV ultrapure water system with a resistivity greater than 18.0 MΩ-cm (Barnstead International). All water purified through this system will hereafter be referred to as nanopure water. Solid AE was purchased from Dr. James Kiddle (Western Michigan University). Catalase (from bovine liver, > 35,000 U mg protein⁻¹, suspension in water containing 0.1% thymol), 3-(2-pyridyl)-5,6-diphenyl-1,2,4-triazine-p,p'-disulfonic acid monosodium salt hydrate (Ferrozine), NaHCO₃ (minimum 99.5%), ultrapure HCl, NaOH, HNO₃, Na₂CO₃, and H₂O₂ (30%) were purchased from Sigma-Aldrich. Diethylene triamine pentaacetic acid pentasodium salt 40% aqueous solution (DTPA) was ordered through Fisher Scientific. Iron(II) sulfate heptahydrate and manganese(II) chloride tetrahydrate (both 99.999%) were ordered through Alfa Aesar. Stock solutions of AE (500 μM, pH 3.0), H₂O₂ (2.5 mM), catalase (300 kU ml⁻¹), Ferrozine (1 mM, pH 6), and DTPA (10 mM, pH 8) are prepared by dissolution or dilution in nanopure water. These stock solutions are kept in the dark at 4°C when not in use. Additional stock solutions of 3 mM Fe(II) and 3 mM Mn(II) were prepared in nanopure water (pH 2 and 3, respectively) and stored in small volumetric flasks. NaHCO₃ was added to sample matrices as needed. The pH of each stock solution and sample matrix was adjusted with either HCl or NaOH.

Four reagent solutions are employed in all H₂O₂ experiments: 1) AE reagent – 5 μM AE and 25 U ml⁻¹ catalase in nanopure water acidified to pH 3.0 with HCl; 2) buffer – 10 mM Na₂CO₃ and 25 U ml⁻¹ catalase in nanopure water acidified to pH 10.0 with HCl; 3) carrier – 25 U ml⁻¹ catalase in nanopure water; and 4) acid wash – 0.01 M HCl in nanopure water. Catalase is added to the AE reagent, buffer, and carrier at least 10 min prior to other amendments and/or use to ensure low H₂O₂ concentrations (i.e. < 20 nM). The AE reagent and buffer are generally prepared 12 – 18 h prior to use. The carrier is consistently prepared less than 1 h prior to use, as catalase degradation has been observed to occur in room-temperature, neutral pH water on the time-scale of hours. All reagents are kept at room temperature prior to and during use. For

laboratory-based experiments, the AE reagent, buffer, and carrier solutions are prepared in 250 ml volumes. For field-based experiments, where the consumption of reagents may continue for several hours, these reagents are prepared in 1 L volumes. The reagents are always prepared and kept in dark high density polyethylene (HDPE) bottles. The acid wash is prepared in 1 L volumes in clear HDPE bottles. All reagent bottles are regularly soaked in 3% HNO₃ at least overnight and rinsed with nanopure water prior to use.

1.3 Method Setup

A schematic of the FIA system is shown in Figures 1.1a and b. The PMT amplifies the chemiluminescence signal from the flow cell, which is generated by the mixing of AE reagent, buffer, and sample or carrier. As shown in Figure 1.1a, between sample injections the AE reagent is mixed with the carrier solution in the mixing tee, and is then mixed with the buffer in the flow cell in a 1:1:2 ratio, respectively. This mixture of AE reagent, carrier, and buffer provides the baseline signal, which is the [H₂O₂] in the combination of reagents (equivalent to less than 20 nM). Directly after sample injection, the injector valves are switched such that sample in excess of the sample loop volume (500 µl) is sent to waste, while the sample portion to be analyzed is pushed through the system by the carrier solution. As shown in Figure 1.1b, the sample then mixes with the AE reagent in equal volumes, and this sample solution then mixes with the buffer in equal volumes in the flow cell (i.e. sample, AE reagent, and buffer in 1:1:2 ratio, respectively). During the sample injection configuration, acid wash fills a separate 500 µl loop; when the injector valves switch back to between-sample configuration, the acid wash is pushed through the mixing tee and the flow cell. The acid wash helps mitigate the build-up of metal carbonate precipitates in the flow cell, which can interfere with the analysis by catalyzing reduced metal oxidation and H₂O₂ production (Miller et al. 2005).



Figures 1.1a and b. Schematic of the FIA system illustrating the sample filling the sample loop (a) and the injection valve switching to inject the sample into the flow cell for analysis (b), courtesy of Waterville Analytical.

1.4 Chemiluminescence Mechanism

The chemiluminescence generating reaction between acridinium ester compounds and H_2O_2 was discovered as early as the 1960's (Kaltenbach and Arnold 1992). The reaction mechanism between AE (the specific acridinium ester employed in the AE-CL method) is outlined by Cooper et al. (2000) and is shown in Figure 1.2. Briefly, the conjugate base of H_2O_2 (HO_2^-) attacks the carbonyl α carbon. Alkaline conditions then abstract the remaining HO_2 -R hydrogen, leading way to the formation of an unstable dioxetane intermediate, which decays to N-methylacridone and light with a maximum wavelength of 470 nm. Because the attacking

species is the peroxide anion (pK_a of H_2O_2 is 11.62) and alkaline conditions enhance the formation of the dioxetane intermediate, the reaction must be carried out at high pH. Over the course of several optimization experiments, a buffer pH of 10.0 was shown to result in both the sensitivity and the analytical range required for freshwater H_2O_2 analysis. Previous studies have investigated the response of the AE-CL method to organic peroxides, but no significant interferences were observed (Miller et al. 2005, King et al. 2007).

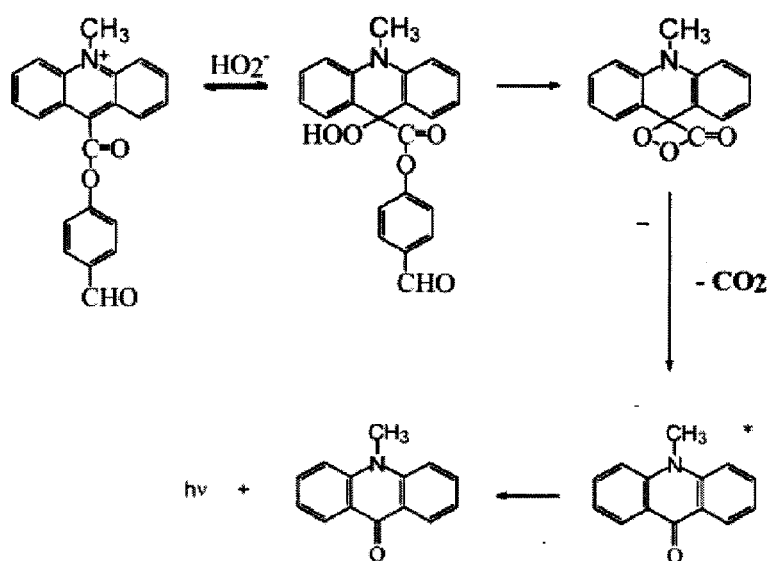


Figure 1.2. Chemiluminescence-generating reaction mechanism exploited in the AE-CL method (Cooper et al. 2000).

1.5 Reagent Stability

Hydrolysis reactions can limit the sensitivity and shelf-life of the AE reagent solution. In a study conducted by Kaltenbach and Arnold (1992), the hydrolytic degradation of a similar acridinium ester compound was monitored at 1 h, 1 d, and 1 wk following preparation of various 140 μ M reagent solutions at pH 3 – 10. Based on high pressure liquid chromatography (HPLC) separation of the various degradation products, Kaltenbach and Arnold concluded that an acridinium ester stock solution should be adjusted to pH 3 for long term viability. Additionally,

by monitoring the decay of the chemiluminescence signal with time under various pH conditions, King et al. (2007) concluded that the pseudo-first-order basic hydrolysis rate constant (k_{OH}) of AE at 25°C is $2.2 \times 10^2 \text{ M}^{-1} \text{ s}^{-1}$, indicating an AE half-life shorter than 9 h above pH 7. The rate of basic hydrolysis concluded by King agrees well with that determined by Littig and Nieman (1993) in a similar study ($2.0 \times 10^2 \text{ M}^{-1} \text{ s}^{-1}$). Thus, AE solutions, both the concentrated stock solution (500 μM) or the more dilute reagent solution (1 μM), should be prepared at pH 3 for reliable use.

Interestingly, King et al. (2007) also concluded the pH-independent water hydrolysis rate constant ($k_{\text{H}_2\text{O}}$) of AE at 25°C to be $8 \times 10^{-5} \text{ s}^{-1}$, which equates to a maximum half-life of just 2.4 h regardless of pH conditions. The author then stated that a pH 3 AE stock solution stored in the refrigerator remained stable for several months. Although this latter conclusion is in agreement with our observed behavior of AE stock solutions (500 μM , pH 3), we also observed that the more dilute AE reagent (1 μM , pH 3) provided consistent, sensitive response for at least 8 h of continuous use at room temperature and remained stable for at least 6 h at temperatures up to 32°C. Additionally, we determined that an AE reagent prepared at least 12 h prior to use provided an equally sensitive response to one prepared directly prior to use, but also yielded much better consistency in sensitivity over the course of several hours.

Lastly, both the AE stock solutions and AE reagents should be acidified to pH 3 with ultrapure HCl. A check of the AE reagent stability with time, by running multiple standard calibrations (see section 1.7) over the course of several hours, revealed that an AE reagent prepared with lower-purity HCl yielded inconsistent and irregular sensitivities. This phenomenon is not observed when the AE reagent, and AE stock solution diluted to make the reagent, is acidified with ultrapure HCl.

1.6 Method Calibration and Chelator Use

To calibrate the AE-CL method, H_2O_2 stock solutions (2.5 mM) are prepared and standardized using the H_2O_2 molar absorptivity of $38.1 \pm 1.4 \text{ M}^{-1} \text{ cm}^{-1}$ at 240 nm (Miller and Kester 1988). The stock solution is placed in a 1 cm quartz cuvette and the absorbance is measured using a Hewlett Packard 8453 UV-VIS photodiode array spectrophotometer. From several standardizations, it was determined that each stock solution was stable for several months when stored in the dark at 4°C .

A $10 \mu\text{M}$ H_2O_2 working stock is prepared directly prior to every standard additions calibration. Calibrations are performed by spiking an appropriate volume of H_2O_2 working stock into a 3 ml plastic Luer-lock syringe containing 2.0 ml of the sample matrix water, inverting the syringe five times for adequate mixing, and injecting the standard into the sample port of the injection valve (refer to Figures 1.1a and b). Note: the amount of working stock spiked into the matrix water accounts for the dilution of H_2O_2 caused by the additional volume of the spike (i.e. for a 500 nM standard, 222 μl of working stock is added to 2 ml matrix, not 200 μl). For freshwater experiments, calibrations generally encompass 0 – 1000 nM H_2O_2 , and consist of two to three separate standard additions and an unamended sample matrix injection (i.e. the “base” injection). An example freshwater standard additions calibration with each $[\text{H}_2\text{O}_2]$ in duplicate is plotted in Figure 1.3.

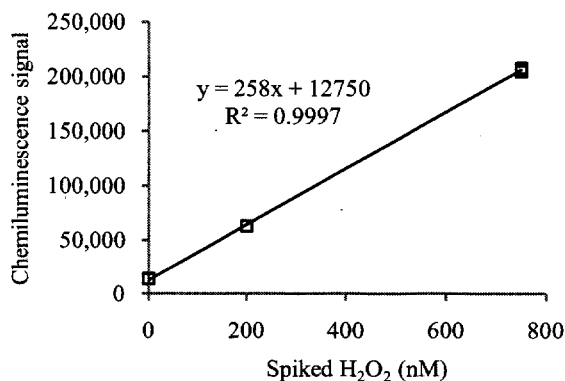


Figure 1.3. Standard additions calibration in a sample matrix of 0.2 μm filtered stream water.

Standard additions calibrations are performed at least every 2 h during continuous analyses to quantify the method sensitivity and to track any changes in sensitivity with time. When the AE reagent is prepared at least 12 h prior to use, the method sensitivity remains consistent for up to 8 h of continuous use at room temperature. For laboratory-based experiments with nanopure water as the sample matrix, the method sensitivity remains constant within $\pm 5\%$. For field-based experiments with natural freshwater as the sample matrix and surrounding air temperature variability, the method sensitivity fluctuates more but generally remains within $\pm 15\%$. In the field, it is important to run standard additions calibrations several times throughout a multiple-hour experiment to ensure that sample measurements are accurately quantified. If the sensitivity consistently decreases with time, samples should be quantified with the most recent calibration. If the sensitivity fluctuates randomly, then either the most recent calibration can be used, or an average sensitivity of all calibrations can be used.

Additionally, to ensure an absence of positive interferences in the sample matrix, blank measurements are regularly conducted by adding 25 U ml^{-1} catalase to the sample matrix, and allowing 10 min in the dark before measurement. Due to the abundance of Fe(II) and Mn(II) in natural freshwaters (Stumm and Morgan 1996), AE-CL interferences from these species are regularly encountered in freshwater measurements. In alkaline conditions like those imposed in the FIA flow cell, these reduced metals (generally present in nanomolar to micromolar concentrations) rapidly oxidize and produce significant concentrations of H_2O_2 (King 1998, Nico et al. 2002). When these species are present in the sample matrix, blank measurements yield AE-CL peaks, characteristically broad, since the activity of catalase cannot compensate for the rapid rates of H_2O_2 production in the flow cell. To eliminate the interference from Fe(II), the complexing agent Ferrozine is spiked into sample syringes. The use of Ferrozine to prevent interfering H_2O_2 production in the FIA system is discussed in Cooper et al. (2000). Although previous studies have either stated or concluded that Mn(II) is very stable in the presence of O_2 under neutral pH conditions (Diem and Stumm 1984), the presence of carbonate and/or hydroxide

ligands in alkaline conditions enhance the oxidation rate of Mn(II) (Morgan 2005). To complex Mn(II) and eliminate its interfering oxidation in the FIA, DTPA is also spiked in sample syringes. The multidentate binding nature of DTPA (Byegard et al. 1999) encloses Mn(II) such that its oxidation and subsequent H₂O₂ production are prevented. For freshwater measurements, Ferrozine and DTPA are each added to sample syringes (in the order mentioned) in 100 μM final concentrations. With these amendments to the appropriate sample matrices, the blank signal is generally equivalent to baseline, and sensitivities are within ± 10% of that observed in nanopure water, indicating an absence of interferences.

The utility of employing Ferrozine and DTPA to complex Fe(II) and Mn(II) in conditions representative of freshwater systems was investigated prior to employing the chelators in field experiments. For this investigation, the sample matrix was 0.5 mM NaHCO₃ (pH 7.5) containing 10 μM Mn(II) and 100 μM Ferrozine, and individual sample syringes were spiked with 5 μM Fe(II) and 100 μM DTPA. Both Mn(II) and Ferrozine are stable in neutral pH solutions, and were thus mixed in with the bulk sample matrix. In contrast, Fe(II) rapidly oxidizes even at neutral pH (King 1998), and was thus spiked into individual syringes. DTPA was also spiked into individual syringes, since Fe(II) must be allowed to complex with Ferrozine in the absence of DTPA. We observed that if Fe(II) is exposed to Ferrozine and DTPA simultaneously, the DTPA competes for binding but the Fe(II)-DTPA complex is rapidly oxidized by O₂ (i.e. interfering Fe(II)-induced peaks observed during AE-CL analysis). After each sample syringe was spiked with Fe(II) and DTPA (in the order mentioned), known [H₂O₂] were added. Figure 1.4 displays the results of this experiment. As shown, measured [H₂O₂] in replicates containing just the chelators (i.e. Fz + DTPA) and replicates containing the metals and chelators (i.e. Metals + Fz + DTPA) agree within 5 nM of spiked [H₂O₂]. Samples containing Mn(II) but no DTPA exhibited the characteristic H₂O₂ production in the flow cell. This data supports the use of DTPA, in conjunction with Ferrozine, to measure H₂O₂ by the AE-CL method in natural freshwaters containing the Mn(II) and Fe(II) metal ions. Note: to reduce the technical complexity of this

experiment, Ferrozine was added to the bulk sample matrix; however, in field experiments, 100 μM Ferrozine is spiked into individual sample syringes, followed by 100 μM DTPA.

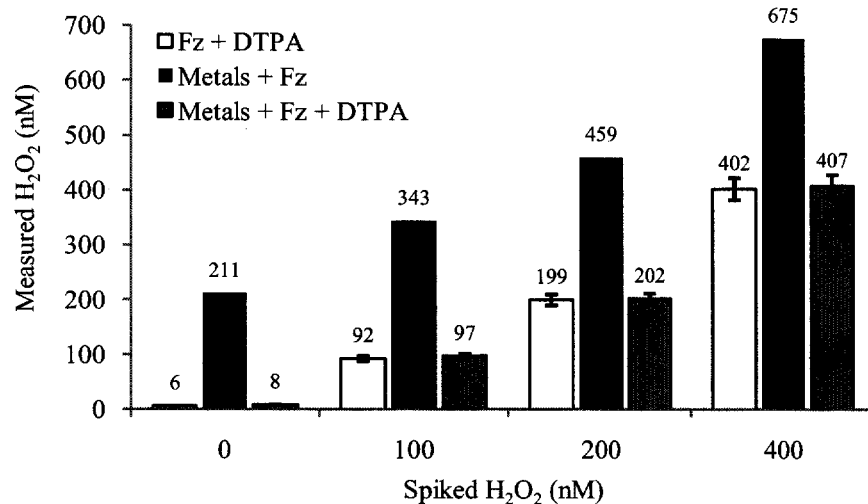


Figure 1.4. Effects of the addition of 5 μM Fe(II), 10 μM Mn(II), 100 μM Ferrozine, and 100 μM DTPA on AE-CL measured $[\text{H}_2\text{O}_2]$.

1.7 Method Precautions for Freshwater Systems

Previous co-worker Dr. Andrew Vermilyea worked with the AE-CL method for several years, and describes several precautionary measures to be taken when preparing the reagents in his Ph.D. dissertation (Vermilyea 2009). Additionally, applying the AE-CL method to natural freshwater systems may require the following precautionary measures. As mentioned in section 1.6, Ferrozine and/or DTPA may be necessary additions to the sample matrix to chelate Fe(II) and other reduced metal species, which can otherwise result in significant interference. Also, because freshwater systems are generally characterized by higher buffering capacity than purified or marine waters, the buffer solution may in turn require a higher buffering capacity to ensure high pH in the flow cell. This issue is readily detected by low calibration sensitivity, and can be mitigated by preparing the buffer with up to 50 mM Na_2CO_3 .

Lastly, because freshwater systems inherently contain more suspended solids and biota than purified and marine waters, it is crucial that filtration is applied to samples and standard additions in order to minimize build-up in the FIA system. In all freshwaters, 0.2 μm polyethersulfone (PES) filters are used either during sample collection or just prior to sample injection in the FIA system. However, it was observed that initial 2 ml aliquots of nanopure water passed through PES filters contained up to 1 μM H_2O_2 more than the same water measured unfiltered. This interference can be eliminated by rinsing all new filters with 10 ml 0.01 M HCl followed by 10 ml MQ prior to use. When the filters are pretreated in this manner, measurements of unfiltered and filtered control solution aliquots indicate a difference in H_2O_2 of < 3%, which is within experimental error.

CHAPTER 2

HYDROGEN PEROXIDE DYNAMICS IN AN AGRICULTURAL HEADWATER STREAM: EVIDENCE FOR SIGNIFICANT BIOLOGICAL PRODUCTION

Hydrogen peroxide (H_2O_2) is known to play key roles in aquatic systems, including metal redox cycling and degradation of organic matter into bioavailable forms. Detailed knowledge of the cycling of H_2O_2 in natural waters thus fosters the understanding of important aquatic biogeochemical processes. Although biological production of H_2O_2 has been observed in culture studies, the significance of this process to the H_2O_2 budget in freshwater systems remains unknown. In this study, isotopically-labeled H_2O_2 ($\text{H}_2^{18}\text{O}_2$) was added to novel in-stream mesocosm systems exposed to light and dark periods. By measuring total H_2O_2 and $\text{H}_2^{18}\text{O}_2$ in tandem, we inferred absolute rates of H_2O_2 production and decay, which were occurring simultaneously. This investigation is the first to characterize absolute rates of freshwater H_2O_2 production *in situ*, and suggests biological production as the dominant control on the H_2O_2 budget in the agricultural headwater stream studied. Further, the results indicate rates of H_2O_2 production up to several-fold the photo-production rates observed in filtered water samples, supporting the need for *in situ* measurements to understand surface water H_2O_2 cycling.

2.1 Introduction

Because of its reactive nature and ability to act as a reductant and an oxidant (Moffett and Zafiriou 1990), hydrogen peroxide (H_2O_2) is an important component of natural waters. Together with the precursor superoxide radical ($\text{O}_2^{\cdot-}$) and byproduct hydroxyl radical (OH^{\cdot}), H_2O_2 is involved in a suite of environmental processes, including biogeochemical metal redox cycling (Sunda et al. 1983, Cooper et al. 1994, Vermilyea and Voelker 2009), and conversion of organic contaminants and natural organic matter into bioavailable forms (Southworth and Voelker 2003, Pullin et al. 2004). Additionally, H_2O_2 has been observed to affect the growth and health of

aquatic micro- and macrobiological communities (Collen et al. 1995, Twiner and Trick 2000, Bischof et al. 2003). Detailed knowledge of H₂O₂ cycling in natural waters is thus critical to understanding a wealth of aquatic biogeochemical processes.

In surface waters, H₂O₂ concentrations ([H₂O₂]) typically follow a diurnal cycle, with the highest concentrations reached during mid-day and the lowest during late night (Cooper and Lean 1989, Richard et al. 2007). H₂O₂ is produced abiotically in sunlight via photo-oxidation of chromophoric dissolved organic matter (CDOM) (Cooper et al. 1994). Reported rates of abiotic photo-production of H₂O₂ in filtered surface waters are typically 10² – 10³ nM h⁻¹ under mid-day irradiance, and decrease proportionally to diminishing sunlight (Cooper et al. 1988, Cooper and Lean 1989, Richard et al. 2007). These observations have led to the conventional assumption that abiotic photo-production is the main source of H₂O₂ in surface waters (Cooper et al. 1994).

However, biological production of H₂O₂ could also be significant. Spurred by H₂O₂'s potentially harmful effects on cell health, efforts to unravel the mechanisms of its biological production began decades ago (Patterson and Myers 1973, Draper and Crosby 1983, Fridovich 1986a). Aquatic photosynthetic organisms (i.e. green algae, cyanobacteria, and other phytoplankton) produce H₂O₂ in chloroplasts according to the Mehler reaction, in which O₂ is utilized as an electron acceptor, forming first superoxide radical (O₂^{•-}), and then H₂O₂ via O₂^{•-} dismutation (Mehler 1951). H₂O₂ is also produced in chloroplasts via photorespiration, in which various substrates are oxidized (i.e. glycolate to glyoxylate) by oxidase enzymes (Asada and Takahashi 1987). Although one might expect that all H₂O₂ formed intracellularly would be rapidly degraded by catalases and peroxidases, because it readily passes through cell membranes (Buettner et al. 2009), H₂O₂ can be excreted by cells. Excretion of biologically photo-produced H₂O₂ into surrounding media has been reported for spinach chloroplasts (Steiger and Beck 1981) and several species of cyanobacteria (Patterson and Myers 1973, Roncel et al. 1989, Park et al. 1991). Additionally, Zepp et al. (1992) conducted an early survey of the governing roles of various freshwater green algae on aqueous [H₂O₂], and observed [H₂O₂] increasing in the

surrounding medium at rates up to $1.7 \mu\text{M h}^{-1}$ in cultures exposed to spring-time sunlight in Athens, Georgia (34°N) (filtered controls to examine photo-production by compounds in the medium were not performed).

Biological production of H_2O_2 can also take place in the dark via extracellular oxidase reactions and intracellular respiration (Fridovich 1986b). Extracellular enzymatic processes contributing to dark H_2O_2 production have been observed in various marine phytoplankton cultures, including *Hymenomonas carterae* and *Chattonella marina* (Palenik et al. 1987, Liu et al. 2007), and ligninolytic fungi (Asada et al. 1986, Paszczyński et al. 1986, Kersten and Kirk 1987). Non-photosynthetic production of H_2O_2 , attributed to intracellular respiration and external enzymatic processes, has been reported in cultures of *Heterosigma akashiwo* (Twiner and Trick 2000). Both *Chattonella marina* and *Heterosigma akashiwo* are infamous for their roles in harmful algal blooms, which are toxic to marine ecosystems due at least in part to their production of the reactive oxygen species $\text{O}_2^{\cdot -}$ and H_2O_2 (Twiner and Trick 2000, Liu et al. 2007).

While the conventional understanding is that abiotic processes dominate the production of H_2O_2 in freshwaters, biological processes are cited as significant controls on H_2O_2 decay (Cooper and Lean 1989, Cooper and Zepp 1990). Zepp et al. (1992) measured the decay of H_2O_2 in dark cultures of various freshwater algae and observed a median half-life of just 1.5 h. Other studies have reported half-lives on the order of hours in unfiltered freshwaters incubated in the dark, whereas the rates of decay in filtered controls were at least an order of magnitude slower (Cooper and Zepp 1990, Richard et al. 2007).

In contrast to culture media, abiotic (i.e. mineral) particles are also present in unfiltered freshwaters. Temporal measurements of $[\text{H}_2\text{O}_2]$ in the presence of pure mineral surfaces have indicated rapid H_2O_2 decay rates (Kwan and Voelker 2002, Scott et al. 2002). Thus, because of the combination of microbiota and minerals, H_2O_2 is quickly decomposed in the presence of sediments and soils (Cooper and Zepp 1990, Petigara et al. 2002). In studies conducted by Cooper and Zepp (1990) and Petigara et al. (2002), sterilized soil suspensions exhibited slower

rates of decay than unsterilized suspensions. However, the significance of biological activity to the rates of decay varied with soil type. In a generally sense, then, both mineral surface-catalyzed and biologically-mediated decay are likely important processes in shallow freshwater systems, where the sediment-water interface could have a large influence.

According to the observed rates of decay, in the absence of production processes $[H_2O_2]$ should reach zero in most freshwater systems after several hours in the dark. However, temporal measurements of $[H_2O_2]$ in unfiltered freshwater incubations and *in situ* have indicated non-zero steady-state $[H_2O_2]$ during the night (Cooper and Lean 1989, Richard et al. 2007, Vermilyea et al. in press), illustrating that dark production mechanisms are balancing decay. Given the aforementioned abundance of enzymatic reactions producing H_2O_2 , many previous studies have suggested that dark production in freshwaters is primarily due to biological processes (Cooper and Lean 1989, Richard et al. 2007, Vermilyea et al. in press). Abiotic production of H_2O_2 can also occur in the dark via thermal reduction of Fe(III) and subsequent oxidation of Fe(II) by O_2 (Pullin and Cabaniss 2003). The concentration of H_2O_2 that can accumulate via this mechanism is limited by simultaneous consumption of H_2O_2 by reaction with Fe(II), and can be calculated from the conditional rate coefficients of the reactions of Fe(II) with O_2 and H_2O_2 (i.e. 40 to 70 nM in air-saturated 10 mM carbonate solutions at pH 7 to 8, respectively; King and Farlow 2000). Although Fe(III) oxyhydroxides may be thermally reduced at significant rates in circumneutral waters containing natural organic matter (NOM) (Pullin and Cabaniss 2003), suggesting that Fe(II) oxidation may be a non-negligible mechanism of dark H_2O_2 production, overnight *in situ* measurements of both $[H_2O_2]$ and $[Fe(II)]$ are needed to elucidate the significance of these processes to freshwater systems, and have so far not been performed (Vermilyea and Voelker 2009).

No studies to date have fully characterized the significance of dark biological H_2O_2 production in freshwater systems due, in part, to the ubiquitous use of sample incubations instead of *in situ* measurements. The latter is inherently complicated by advective H_2O_2 transport as well

as competing production and decay processes (Shtamm et al. 1991, Vermilyea et al. in press). For these reasons, samples are generally collected and incubated in bottles, where irradiance is controlled, advective fluxes of H_2O_2 are insignificant, and one can either allow production and decay contributions by biota or eliminate them via filter-sterilizing. However, incubating freshwater samples fails to incorporate all naturally occurring processes governing $[\text{H}_2\text{O}_2]$ *in situ*, such as the effects of biofilms and mineral surfaces on an undisturbed sediment-water interface. For example, notably faster rates of decay have recently been reported in stream water incubations containing biofilm-covered terracotta tiles with respect to incubations in the absence of films (Richard et al. 2007). The role of algal biofilms as a significant source of biological production has not yet been investigated.

An additional limitation of previous freshwater studies is that only total $[\text{H}_2\text{O}_2]$ was measured, and thus only the net results of simultaneously occurring decay and production processes were observed. For example, typical dark incubation studies fit total $[\text{H}_2\text{O}_2]$ data with first-order plots to determine a first-order dark decay coefficient, and disregard the possibility of simultaneous production (Richard et al. 2007). If significant dark production is in fact occurring, this approach results in an underestimate of the true decay coefficient, and thus of the turnover of H_2O_2 in freshwater systems. This is illustrated in a recent study by Vermilyea et al. (in press), where H_2O_2 and an added isotope-labeled tracer, $\text{H}_2^{18}\text{O}_2$, were measured simultaneously in incubations of several unfiltered lake water samples, allowing for quantification of absolute as well as net decay rates. The study determined that net decay rates were only about 30% of the absolute decay rates due to dark production of H_2O_2 , which was calculated to occur at rates of 29 – 122 nM h^{-1} . Such rates are significant in comparison to abiotic photo-production (which only occurs in near-surface waters) when averaged over 24 h throughout the depth of the water body.

In the study reported here, we aimed to expand on the isotope-labeled tracer methodology to investigate the H_2O_2 budget in a natural freshwater system, including the importance of biological communities present both in the water and at the sediment-water interface. Novel

mesocosm systems were installed in Maple Creek, a shallow agricultural headwater stream in eastern Nebraska. Closed-bottom mesocosms (i.e. controls) were utilized to investigate the processes occurring in the stream water, and opened-bottom mesocosms (with equilibrated downward flow to prevent hyporheic upwelling) were employed to examine the additional impacts of the sediment-water interface. Controlled *in situ* measurements of $[H_2O_2]$ and $[H_2^{18}O_2]$ were collected in both mid-day light and complete darkness, allowing for resolution of absolute rates of decay, photo-production, and dark production.

2.2 Methods

In this section, we discuss the two analytical methods, the AE-CL method for total H_2O_2 analysis and the $H_2^{18}O_2$ method, as well as the materials, sampling scheme, and calibration/quality control techniques, utilized for measuring $[H_2O_2]$ and $[H_2^{18}O_2]$ in an *in situ* freshwater system. We also describe the location of the field site investigated in this study, and detail all required field equipment to conduct the *in situ* measurements. Please refer to Chapter 1 for details regarding the AE-CL method materials, equipment, use, calibration, and precautions.

2.2.1 $H_2^{18}O_2$ Method

The method of analysis for $H_2^{18}O_2$ concentrations is described in detail in Vermilyea et al. (in press). Briefly, $H_2^{18}O_2$ was oxidized to $^{18}O_2$ immediately after sampling by an organic-Cu(II) complex, following purging with ultra-pure helium. Sodium azide was used to preserve the samples, which were stored inverted in a dark, ice-chilled cooler until $^{18}O_2$ could be quantified using gas chromatography-mass spectrometry (GC-MS) analysis, which took place within 5 d of sampling. Vermilyea et al. (in press) report that samples treated and stored in this manner remained stable for at least 6 d. Refer to section 2.2.5 for more details regarding $H_2^{18}O_2$ sample collection, preparation, and analysis.

2.2.2 Materials for H₂¹⁸O₂ Method

Bathocuproine (2,9-dimethyl-4,7-diphenyl-1,10-phenanthroline), Cu(II)Cl₂ (reagent grade), and sodium azide were ordered through Sigma Aldrich. The H₂¹⁸O₂ stock solution was synthesized from ¹⁸O₂ gas (ISOTEC, random 97 atom % ¹⁸O) according to the method described in Grassi et al. (2002). Refer to Vermilyea et al. (in press) for details regarding the synthesis of the stock solution used in this study. The H₂¹⁸O₂ stock solution was analyzed for both total [H₂O₂], using the AE-CL method and by checking the absorbance at 240 nm (as described in Chapter 1), and [H₂¹⁸O₂] according to the procedure described in section 2.2.1. The concentration of total H₂O₂ measured via the AE-CL method agreed with that obtained by measuring the absorbance within ± 5%, and yielded a stock concentration of 0.06 M. Measurements of [H₂¹⁸O₂] in the stock solution yielded a 95:5 ratio of isotopically-labeled to total H₂O₂, respectively. Refer to Vermilyea et al. (in press) for details regarding measuring [H₂¹⁸O₂] in the stock solution.

2.2.3 Site Location

During 22 and 23 August 2009 (hereafter referred to as day 1 and day 2), we conducted two field experiments 250 m upstream from the United States Geological Survey (USGS) gauging station 06800000 (latitude 41°33'37", longitude 96°32'27") in Maple Creek, near Nickerson, Nebraska. The Maple Creek watershed is a 955 km² watershed with its land use dominated by agriculture (95%) (Capel et al. 2008). Maple Creek has been identified and investigated by the USGS under the National Water-Quality Assessment Program in recent years as a representative agricultural headwater stream impacted by farm-based chemicals (Fredrick et al. 2006). The stream is characterized by shallow annual mean flows (2.27 m³ s⁻¹), sediment composed of fine sand and silt, and high nutrient loads (Fredrick et al. 2006, Puckett et al. 2008). The site was chosen for our field-based experiments due to flow and sediment conditions conducive to *in situ* surface water sampling, availability of water quality data, real-time gauging

station data, and nutrient and temperature conditions favorable to biotic activity (Puckett et al. 2008).

2.2.4 Experimental Setup

To investigate the dynamics of H_2O_2 in Maple Creek, we measured $[\text{H}_2\text{O}_2]$ and $[\text{H}_2^{18}\text{O}_2]$ in mesocosms subjected to mid-day sunlight and complete darkness. The input concentrations and residence times of H_2O_2 and $\text{H}_2^{18}\text{O}_2$ were separately controlled in each mesocosm, and black plastic tarps were used to control the timing and duration of sunlight irradiance. The mesocosms are hollow cylinders made of Solacryl® SUVT (Spartech Company), UV-transparent plexiglass, 0.64 cm thick, standing 61 cm tall, with inner diameters of 46 cm. Solacryl® SUVT is transparent to both visible and UV light; these properties were verified by checking light transmittance on a Hewlett Packard 8453 UV-VIS photodiode array spectrophotometer prior to the field experiments.

Two of the mesocosms were open-ended on both top and bottom, whereas the other was closed-bottom (i.e. bottom opening sealed with same material). The closed-bottom control (MC) was utilized in tandem with the two opened-bottom mesocosms (M1 and M2) to discern the processes imposed by the sediment-water interface from those occurring in the stream water. The mesocosms were positioned in shallow water next to a gentle sandbar. M1 and M2 were forced 20 cm into the stream sediment. MC was placed near M1 and M2, but in slightly shallower water to prevent it from being moved by the stream current.

Two sets of tubing were placed on the inner walls of each mesocosm to deliver input water (Figure 2.1). In M1 and M2, the input water exited down through the sediment and prevented hyporheic upwelling. The combined flow rate of the input water was adjusted to provide a steady head just slightly higher than the depth of water in the surrounding portion of the stream (i.e. 12 – 15 cm). The water depth in MC was controlled by placing the end of tubing (Masterflex C-FLEX, 6.35 mm ID) attached to an outwardly directed peristaltic pump at the

height desired; thus, water in excess of the desired depth was rapidly pumped out. The depths and flow rate of water into each mesocosm was monitored throughout each experimental day. Because the input flow rates and water levels were constant and known, the residence time (T_r) in each mesocosm could be calculated as (Dingman 2002):

$$T_r = \frac{V_m}{Q_{out}} \quad (2.1)$$

where V_m = water volume in mesocosm, and Q_{out} = volumetric flow rate out of the mesocosm = volumetric flow rate into the mesocosm. With typical water volumes and flow rates of 24 L and 0.08 L min^{-1} , respectively, T_r values were on the order of 5 h. However, due to slight differences in water depths and flow rates, the T_r for each mesocosm was individually calculated.

To ensure that the water volume in each mesocosm was well mixed, a small circulation pump was placed inside each mesocosm just below the water surface and directly under the input water tubing. The circulation rate and placement were chosen to maximize mixing in all mesocosms while minimizing sediment resuspension in M1 and M2. A simple rhodamine dye test was conducted in MC prior to setting up for field experiments to verify that complete mixing of input water was obtained within 20 s of addition. This effectively eliminated any diffusion-controlled effects in the mesocosms.

The mesocosm input water was delivered from two sources: reservoir and injectate. The reservoir water was Maple Creek surface water, $10 \mu\text{m}$ filtered to remove large algae and sediments that might clog the sample lines. Approximately 400 L of reservoir water was placed in a plastic tank the night before each experiment, and was kept covered with an opaque tarp to minimize H_2O_2 photo-production (which would change input $[\text{H}_2\text{O}_2]$) during each experimental day. Due to a small leak, up to 100 L of filtered stream water was added to the reservoir tank the morning of each experiment to ensure an adequate supply of reservoir water. The injectate

consisted of distilled water containing $4 \mu\text{M H}_2^{18}\text{O}_2$ (prepared fresh every morning), housed in distilled water container in a shaded area. The reservoir water was delivered to each mesocosm in clear vinyl tubing (6.35 mm ID) at approximately 75 ml min^{-1} . Black Norprene tubing (1.59 mm ID) delivered the injectate water to each mesocosm at approximately 7.5 ml min^{-1} . The reservoir and injectate pumps were adjusted for each mesocosm separately to account for slight differences in water depths. The concentration of $\text{H}_2^{18}\text{O}_2$ in the injectate was chosen such that the ten-fold dilution when mixed with the reservoir water yielded an input mesocosm concentration of 400 nM. Total H_2O_2 concentrations in the reservoir water were 100 – 200 nM, yielding total $[\text{H}_2\text{O}_2]$ input of 500 – 600 nM (i.e. $\text{H}_2^{18}\text{O}_2 + \text{H}_2\text{O}_2$).

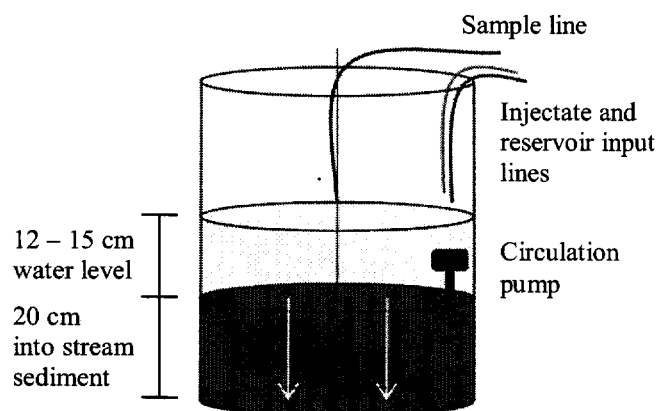


Figure 2.1. Depiction of in-stream opened-bottom mesocosm setup (i.e. M1 and M2). Arrows indicate direction of water flow (i.e. down through sediment). Closed-bottom controls (i.e. MC) were setup in a similar fashion, but with the addition of an outlet line opposite to the circulation pump. Also, closed-bottom controls were not forced into the stream sediment.

The reservoir lines continuously pumped water into M1 and M2 throughout the night before each experimental day to induce an equilibrated downward flow state. Upon arrival to the field site each morning (i.e. 8:00 – 9:00), MC was filled with approximately 24 L of reservoir water, the MC reservoir and outlet pumps were started, and all circulation pumps were powered on. Additionally, each mesocosm was covered upon arrival to eliminate photo-production of H_2O_2 and thus enable lower initial $[\text{H}_2\text{O}_2]$ for the experiments. The injectate pumps were

powered on and each mesocosm was spiked with approximately 200 nM $\text{H}_2^{18}\text{O}_2$ at least 1 h prior to uncovering the mesocosms. The time between beginning injectate input (and spiking) and uncovering was utilized to sample for $[\text{H}_2^{18}\text{O}_2]$ and $[\text{H}_2\text{O}_2]$. After $[\text{H}_2\text{O}_2]$ appeared to steady, the mesocosms were uncovered and exposed to sunlight for several hours to induce photo-production. A Solar Light Company model PMA2100 photometer was placed on the sandbar within 1 – 2 m of the mesocosms for 1 min resolution UVA (315 – 400 nm) measurements to enable comparisons between photo-production and sunlight intensity during the mid-day light period. In the mid- to late-afternoon, the mesocosms were again covered to eliminate photo-production and investigate the dynamics of dark H_2O_2 processes.

To enable day to day comparisons, we scrubbed the walls of each mesocosm free of algae between experiments. We also measured the pH in each mesocosm multiple times throughout each day with a Thermo Orion PerpHecT Combination pH electrode attached to a Thermo Orion model 720A pH meter. Additionally, we augmented the injectate of M1 with HCl during day 1, and augmented the injectates of both M1 and MC during day 2, to investigate the pH dependence of decay and production processes. During day 1, the initial pH in M2 and MC was 8.3, and the pH in M1 was 6.6. However, within 1 h of augmenting M1, the pH rose to 7.5 and remained at this value (± 0.2 pH units) throughout the day. The pH in M2 and MC remained at 8.3 (± 0.2 pH units). During day 2, the initial pH in M2 was 8.5, and the pH in M1 and MC was 6.6. Again, shortly after augmenting the pH rose to 7.5 in both M1 and MC, and remained at this value (± 0.3 pH units) throughout the day. The pH in M2 remained at 8.5 (± 0.1 pH units). However, the impacts of amending the pH was undetectable in terms of production processes, and are only evidenced by slightly increased rates of decay (discussed in section 2.5.1).

2.2.5 Sampling and Method Calibration

Both total H_2O_2 and $\text{H}_2^{18}\text{O}_2$ samples were collected from each mesocosm at least every hour. Sampling generally commenced before 12 pm and ended before 9 pm during each

experiment day. Black Norprene sample tubing (1.59 mm ID, ~ 3 m in length) was positioned such that samples were withdrawn from the vertical and horizontal center of each mesocosm. The black Norprene tubing was chosen to hinder algal growth within the line. Sample lines were driven by peristaltic pumps set at 1.5 ml min^{-1} . Each sample line pumped water into sample syringes through in-line $0.2 \text{ }\mu\text{m}$ polyethersulfone (PES) filters to eliminate particle- and biologically-mediated decay while the sample syringes were being filled. Sample filters were used for 1 – 1.5 h and then exchanged for new filters to minimize biotic and particulate build-up. Additionally, new filters were purged with approximately 20 ml of surface water prior to use. The average travel time from the mesocosms to the sample syringes was 4 min.

All total H_2O_2 samples (2.0 ml final volume) were pumped directly into 3 ml plastic syringes containing Ferrozine (placed within the tip of each sample syringe, final concentration $100 \text{ }\mu\text{M}$). DTPA (final concentration $100 \text{ }\mu\text{M}$) was added to the sample syringes directly following sample collection. Care was taken to ensure the final sample volume was 2.0 ml. Because the sensitivity of the AE-CL method varies with the water matrix (i.e. freshwater vs. purified water), calibration curves, where known concentrations of H_2O_2 were spiked into each standard syringe, were obtained in $0.2 \text{ }\mu\text{m}$ filtered surface water with the addition of the metal chelators as described above. These calibration curves were performed approximately once every hour, and indicated that the AE-CL sensitivity remained constant $\pm 10\%$ over the course of each experimental day. Refer to Chapter 1 for details regarding the calibration curves. Additionally, several surface water blanks containing 25 U ml^{-1} catalase were analyzed, and indicated an absence of positive interferences (i.e. blank signals were equal to the baseline signal). Samples of the mixture of injectate and reservoir lines were also analyzed multiple times throughout each experimental day to ensure approximately constant $[\text{H}_2\text{O}_2]$ input into each mesocosm.

Each 6.00 ml $\text{H}_2^{18}\text{O}_2$ sample (filtered in-line as described above) was collected in 10 ml plastic syringes. Immediately following collection, each sample was dispensed into an Exetainer vial (7.5 ml) with inlaid septa screw cap, spiked with 10 mM sodium azide, and tightly sealed.

The vial septum was then pierced with a 22 gauge needle (15 cm length) extending to the bottom of the sample and purged with helium for 4 min. Just prior to the 4 min mark, 0.3 mM (final concentration) bathocuproine was injected through the septum. Directly following the helium purge, 0.1 mM CuCl_2 was injected through the septum to produce the bathocuproine-Cu(II) complex used to oxidize $\text{H}_2^{18}\text{O}_2$ to $^{18}\text{O}_2$. Sample vials were then inverted to limit the diffusion of $^{18}\text{O}_2$ through the septa, and stored in a dark, ice-chilled cooler. At the end of every experimental day, the $\text{H}_2^{18}\text{O}_2$ samples and standards were transferred to a refrigerator. The samples and standards were transported back to the laboratory in a dark, ice-chilled cooler, and were analyzed within 5 d of collection. Refer to Vermilyea et al. (in press) for details regarding quality control checks on the procedures used to collect, prepare, and store $\text{H}_2^{18}\text{O}_2$ samples.

Several quality control standards were also prepared in the field by spiking distilled water with known concentrations of $\text{H}_2^{18}\text{O}_2$ (i.e. 50 – 300 nmol L^{-1}), and treating them in the same manner as all other samples. GC-MS analysis of the standards revealed linear calibration curves ($R^2 = 0.93$) and relative errors of 18%. The 18% error associated with the $\text{H}_2^{18}\text{O}_2$ standard calibration was not considered in the measured samples, as it is small compared to the uncertainty discussed in section 2.4.3.

2.3 Modeling

A series of first-order, linear differential equations were developed to investigate the behavior of $\text{H}_2^{18}\text{O}_2$ and H_2O_2 in the Maple Creek mesocosms. Because the mesocosms remained covered except for about a four-hour period in the middle of each experimental day, they experienced only two light conditions: mid-day irradiance and complete darkness. The differential equations were integrated to generate models describing $[\text{H}_2^{18}\text{O}_2]$ and $[\text{H}_2\text{O}_2]$ as a function of time under the light and dark conditions, and were employed to characterize the decay and production dynamics of H_2O_2 in Maple Creek. It is important to note that the $\text{H}_2^{18}\text{O}_2$ and

H₂O₂ models were utilized as tools to examine the magnitudes of *in situ* decay and production processes, and not to definitively predict concentrations at any given time point.

2.3.1 Modeling the Decay

In order to characterize the absolute rates of H₂O₂ production in the mesocosms, absolute rates of decay must first be determined. Given that the natural proportion of ¹⁸O₂, and thus H₂¹⁸O₂ via ¹⁸O₂ reduction, is ~ 0.0004% (Vermilyea et al. in press), *in situ* production of H₂¹⁸O₂ is insignificant in comparison with input [H₂¹⁸O₂] from the injectate. Thus, measuring [H₂¹⁸O₂] provides the ability to observe absolute rates of decay. Throughout each experimental day, the change in [H₂¹⁸O₂] with time is described with the following first-order differential equation:

$$\frac{d[\text{H}_2^{18}\text{O}_2]_m}{dt} = -k_f([\text{H}_2^{18}\text{O}_2]_m - [\text{H}_2^{18}\text{O}_2]_{in}) - k_d[\text{H}_2^{18}\text{O}_2]_m \quad (2.2)$$

where k_f represents the first-order exchange, or flushing, coefficient (h^{-1}) accounting for input of injectate and reservoir water and export of an equal quantity of mesocosm water to the sediments (or pumped out in the case of MC), k_d represents the first-order decay coefficient of H₂O₂ (h^{-1}), and $[\text{H}_2^{18}\text{O}_2]_m$ and $[\text{H}_2^{18}\text{O}_2]_{in}$ represent the mesocosm surface water concentration and the incoming concentration in the injectate/reservoir mix (i.e. 400 nmol L⁻¹), respectively.

If one assumes k_f , k_d , and $[\text{H}_2^{18}\text{O}_2]_{in}$ to be constant, (2.2) can be integrated to describe $[\text{H}_2^{18}\text{O}_2]_m$ as a function of time:

$$[\text{H}_2^{18}\text{O}_2]_m(t) = \left([\text{H}_2^{18}\text{O}_2]_0 - \frac{k_f[\text{H}_2^{18}\text{O}_2]_{in}}{k_f+k_d}\right) e^{-(k_f+k_d)t} + \frac{k_f[\text{H}_2^{18}\text{O}_2]_{in}}{k_f+k_d} \quad (2.3)$$

where $[H_2^{18}O_2]_0$ for each mesocosm is the measured $[H_2^{18}O_2]$ directly prior to uncovering the mesocosms (i.e. 12:25 for day 1 and 11:28 for day 2, see Figures 2.2c and d). For each mesocosm, k_f was calculated as the inverse of the associated T_r (Martin and McCutcheon 1998) as defined by (2.1), and was assumed constant throughout each day (based on the steady inflow and head in each mesocosm). Refer to section 2.4.1 for a discussion on determining $[H_2^{18}O_2]_{in}$. A statistically valid range of k_d values for each mesocosm was then determined using the Microsoft Excel Solver function to minimize the sum of squared differences between measured and modeled $[H_2^{18}O_2]$. Refer to section 2.4.3 for details regarding determining the range of k_d values for each mesocosm.

2.3.2 Modeling the Dark Production

Because H_2O_2 undergoes simultaneous decay and production, changing $[H_2O_2]$ with time during the afternoon period when the mesocosms were covered (hereafter referred to as the dark period) is described with an equation analogous to (2.2) but with the addition of a dark production term:

$$\frac{d[H_2O_2]_m}{dt} = -k_f([H_2O_2]_m - [H_2O_2]_{in}) - k_d[H_2O_2]_m + P_{dark} \quad (2.4)$$

where P_{dark} ($nM h^{-1}$) represents the rate of dark production, and is the sum of abiotic dark production and dark biological production ($P_{bio,dark}$, $nM h^{-1}$). Two approaches are discussed for modeling dark $[H_2O_2]$: 1) P_{dark} assumed constant, and 2) P_{dark} modeled as exponentially decreasing with time, according to:

$$P_{dark} = Ae^{-bt} \quad (2.5)$$

Integration of (2.4) with respect to time according to the two approaches yields the explicit models (2.6) and (2.7):

P_{dark} constant with time:

$$[\text{H}_2\text{O}_2]_{\text{m}}(t) = \left([\text{H}_2\text{O}_2]_0 - \frac{k_{\text{f}}[\text{H}_2\text{O}_2]_{\text{in}} + P_{\text{dark}}}{k_{\text{f}} + k_{\text{d}}} \right) e^{-(k_{\text{f}} + k_{\text{d}})t} + \frac{k_{\text{f}}[\text{H}_2\text{O}_2]_{\text{in}} + P_{\text{dark}}}{k_{\text{f}} + k_{\text{d}}} \quad (2.6)$$

P_{dark} exponentially decreasing with time according to (2.5):

$$[\text{H}_2\text{O}_2]_{\text{m}}(t) = \left([\text{H}_2\text{O}_2]_0 - \frac{k_{\text{f}}[\text{H}_2\text{O}_2]_{\text{in}}}{k_{\text{f}} + k_{\text{d}}} - \frac{A}{k_{\text{f}} + k_{\text{d}} - b} \right) e^{-(k_{\text{f}} + k_{\text{d}})t} + \frac{A}{k_{\text{f}} + k_{\text{d}} - b} e^{-bt} + \frac{k_{\text{f}}[\text{H}_2\text{O}_2]_{\text{in}}}{k_{\text{f}} + k_{\text{d}}} \quad (2.7)$$

Refer to section 2.4.1 for a discussion on determining $[\text{H}_2\text{O}_2]_{\text{in}}$. The dark period $[\text{H}_2\text{O}_2]_0$ for each mesocosm is the measured $[\text{H}_2\text{O}_2]$ directly prior to covering the mesocosms (i.e. 16:45 for day 1 and 15:00 for day 2, see Figures 2.2a and b). To determine constant P_{dark} or A and b parameters for each mesocosm, the respective k_{d} determined from the $\text{H}_2^{18}\text{O}_2$ data was varied across its range of uncertainty (discussed in section 2.4.3), and best-fit P_{dark} or A and b parameters were calculated for each k_{d} value using the Microsoft Excel Solver function to minimize the sum of squared differences between measured and modeled $[\text{H}_2\text{O}_2]$. The overall best-fit combination of k_{d} , constant P_{dark} , or A and b parameters were chosen as those resulting in the minimum sum of squared differences.

2.3.3 Modeling the Light Production

During the mid-day period when the mesocosms were uncovered (hereafter referred to as the light period), changing $[\text{H}_2\text{O}_2]$ with time in the light is described analogous to (2.4) but with the rate of light production (P_{light} , nM h^{-1}) replacing P_{dark} :

$$\frac{d[\text{H}_2\text{O}_2]_m}{dt} = -k_f([\text{H}_2\text{O}_2]_m - [\text{H}_2\text{O}_2]_{in}) - k_d[\text{H}_2\text{O}_2]_m + P_{light} \quad (2.8)$$

where P_{light} represents the sum of abiotic photo-production (P_{photo} , nM h^{-1}) and biological production ($P_{bio,light}$, nM h^{-1}). Two approaches are discussed for modeling light $[\text{H}_2\text{O}_2]$: 1) constant P_{light} , and 2) P_{light} nonlinearly increasing with time, according to:

$$P_{light} = C + D\sqrt{t} \quad (2.9)$$

Integration of (2.8) with respect to time according to the two approaches yields the explicit models (2.10) and (2.11):

Constant P_{light} :

$$[\text{H}_2\text{O}_2]_m(t) = \left([\text{H}_2\text{O}_2]_0 - \frac{k_f[\text{H}_2\text{O}_2]_{in} + P_{light}}{k_f + k_d}\right) e^{-(k_f + k_d)t} + \frac{k_f[\text{H}_2\text{O}_2]_{in} + P_{light}}{k_f + k_d} \quad (2.10)$$

P_{photo} increasing with time according to (2.9):

$$[\text{H}_2\text{O}_2]_m(t) = \left([\text{H}_2\text{O}_2]_0 - \frac{k_f[\text{H}_2\text{O}_2]_{in} + C}{k_f + k_d}\right) e^{-(k_f + k_d)t} + \frac{k_f[\text{H}_2\text{O}_2]_{in} + C}{k_f + k_d} - \frac{D \int \sqrt{t} e^{t(k_f + k_d)} dt}{e^{t(k_f + k_d)}} \quad (2.11)$$

The light period $[\text{H}_2\text{O}_2]_0$ for each mesocosm is the measured $[\text{H}_2\text{O}_2]$ directly prior to uncovering the mesocosms (i.e. 12:25 for day 1 and 11:28 for day 2, see Figures 2.2a and b). The overall best-fit k_d values determined from modeling the dark period were assumed constant throughout each day (discussed in section 2.4.3), and were thus applied to the light period. Because the last term in (2.11) cannot easily be computed by Microsoft Excel, the Solver function was not utilized to determine best-fit C and D parameters. Instead, the Solver function was used to estimate the C

and D parameters by minimizing the sum of squared differences between measured and modeled $\frac{d[H_2O_2]}{dt}$ using the differential form of (2.11) given by (2.8). Measured $\frac{d[H_2O_2]}{dt}$ was approximated for each time point as the quotient of the difference between measured $[H_2O_2]$ at one time and measured $[H_2O_2]$ at the next time over the time duration separating the measurements. Wolfram Mathematica was then used to calculate $[H_2O_2]$ explicitly with (2.11).

2.4 Results

In this section, we present all relevant data collected during 22 and 23 of August 2009 at the field site in Maple Creek. Along with the flushing coefficients (k_f), the input concentrations ($[H_2^{18}O_2]_{in}$ and $[H_2O_2]_{in}$) and absolute decay constants (k_d) are key parameters in characterizing the absolute rates of *in situ* production. The production processes are first qualitatively explored, and then quantitatively analyzed via the modeling approaches detailed in sections 2.3.1 – 2.3.3.

2.4.1 Input Concentrations and Flushing Coefficients

To ensure that input $[H_2^{18}O_2]$ and $[H_2O_2]$ (i.e. $[H_2^{18}O_2]_{in}$ and $[H_2O_2]_{in}$) were controlled, multiple measurements of the mixture of injectate and reservoir lines (hereafter referred to as input samples) were collected throughout each of the experimental days. Results revealed that $[H_2O_2]_{in}$ slowly decreased, by less than 25% over the course of an experimental day (~ 8 h): 6.5×10^2 nM to 5.0×10^2 nM during day 1, and 5.0×10^2 nM to 4.0×10^2 nM during day 2. A subsequent control experiment focusing on $H_2^{18}O_2$ injectate stability indicated that $[H_2^{18}O_2]_{in}$ remained constant within $\pm 10\%$ over the course of 6 h. We therefore attribute the decrease in $[H_2O_2]_{in}$ to decreasing $[H_2O_2]$ in the reservoir water, and not to decaying $H_2^{18}O_2$ in the injectate. To keep the models as simple as possible, $[H_2O_2]_{in}$ was modeled as remaining constant according to the average of measured incoming samples, and $[H_2^{18}O_2]_{in}$ was fixed at 400 nM. Uncertainties resulting from these simplifications are discussed in section 2.4.3.

It is also important to note that the rate of total H_2O_2 input to the mesocosms was much less than rates of natural H_2O_2 production in Maple Creek. For example, assuming $[\text{H}_2\text{O}_2]_{\text{in}}$ remained at $0.65 \mu\text{M}$ (i.e. the highest concentration measured), and was pumped in at the rate of 0.08 L min^{-1} (i.e. the average input rate), the rate of total H_2O_2 input to the mesocosms equates to just $0.1 \mu\text{M h}^{-1}$ (accounting for the approximately 24 L volume of the mesocosms). This input rate is notably less than photo-production rates in Maple Creek (discussed in section 2.4.6), and thus is assumed to not impact the natural processes occurring in the stream water.

As mentioned in section 2.3.1, the flushing coefficient (k_f) was calculated as the inverse of the residence time (T_r). Table 2.1 lists the k_f and associated H_2O_2 T_r values for all mesocosms. The slight variability in k_f and T_r values is a result of small differences in water levels (i.e. heads) and input flow rates between mesocosms.

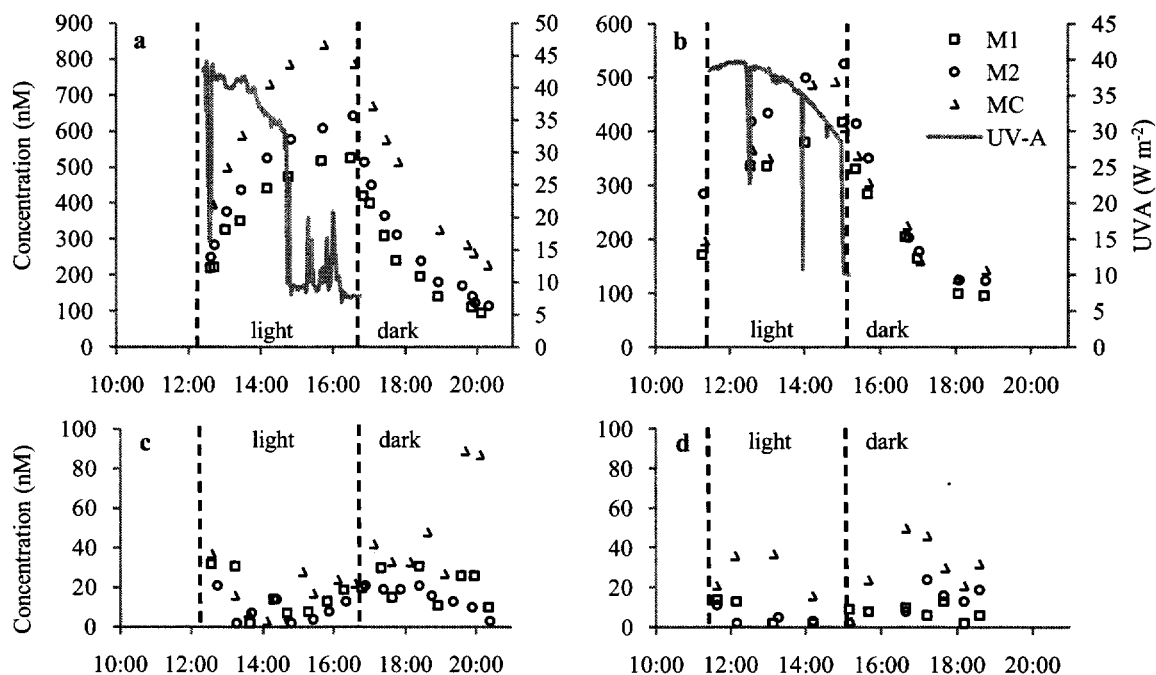
Table 2.1. First-order k_f and associated T_r for each mesocosm. T_r was calculated according to (1), and k_f was calculated as the inverse of T_r .

Day	Mesocosm	k_f (h^{-1})	T_r (h)
1	M1	0.22	4.5
1	M2	0.21	4.8
1	MC	0.21	4.8
2	M1	0.20	4.9
2	M2	0.21	4.7
2	MC	0.21	4.8

2.4.2 Measured Concentrations

As expected, measured $[\text{H}_2\text{O}_2]$ increased during the light period due to photo-production, and subsequently decreased during the dark period on both experimental days (Figures 2.2a and b). The duration of the light period was 12:25 – 16:45 during day 1, and 11:30 – 15:00 during day 2. During the light periods, $[\text{H}_2\text{O}_2]$ increased nonlinearly, appearing to plateau just prior to covering. The subsequent decay of H_2O_2 during the dark periods follows an apparent first-order

trend. In contrast to total $[H_2O_2]$, measured $[H_2^{18}O_2]$ rapidly decreased following the initial ~ 200 nM spike, and remained below 40 nM in M1 and M2, and below 80 nM in MC throughout the duration of the experimental days (Figures 2.2c and d).



Figures 2.2a – d. Measured $[H_2O_2]$ (a and b) and $[H_2^{18}O_2]$ (c and d) during days 1 and 2. The early morning time periods were also in the dark.

2.4.3 Decay Coefficients

As indicated in Figures 2.2c and d, absolute decay rates were fast and resulted in low $[H_2^{18}O_2]$ following the initial morning dark period (during which the mesocosms were equilibrating with the input and spiked concentrations). Based on this behavior, a statistical range of k_d values for each mesocosm was determined via (2.3), assuming a given k_d value remained constant throughout the light and dark periods. The statistical range of a given k_d was determined by applying a 90% confidence interval to the average of measured $[H_2^{18}O_2]$ ($n > 10$) and calculating high and low k_d values resulting in the lower and upper confidence interval

concentrations, respectively. Table 2.2 lists the 90% confidence interval $[H_2^{18}O_2]$, as well as the steady-state $[H_2^{18}O_2]$ associated with the overall best-fit k_d value, for each mesocosm. As discussed in section 2.3.2, the overall best-fit k_d value for each mesocosm was that which resulted in the best fits to measured $[H_2^{18}O_2]$ and $[H_2O_2]$, accounting for production processes, during the dark period (discussed in sections 2.3.2 and 2.4.5). Due to model complexity (see section 2.3.3), light period $[H_2O_2]$ and production terms were not used to calculate the overall best-fit k_d ; instead, the k_d determined using dark period $[H_2O_2]$ and production terms was assumed constant throughout the day. Figure 2.3 displays the results of this analysis, which indicate half-lives of just 0.05 – 0.20 h in M1 and M2, and 0.18 – 0.47 h in MC. While there may be temporal trends in the $[H_2^{18}O_2]$ data (i.e. lower $[H_2^{18}O_2]$, indicating faster decay, in the light, and two points suggesting increasing $[H_2^{18}O_2]$ at the end of day 1 in MC), these were of similar magnitude as the scatter in the data and were thus neglected in this analysis. Refer to section 2.5.1 for a discussion on assuming non-constant k_d values.

Table 2.2. Steady-state $[H_2^{18}O_2]$ associated with the overall best-fit k_d value and 90% confidence interval $[H_2^{18}O_2]$ used to calculate uncertainty in k_d . All concentrations listed are in nM.

Day	Mesocosm	Steady-state	Low	High
1	M1	15	11	18
1	M2	16	12	19
1	MC	39	28	50
2	M1	12	6	14
2	M2	15	8	18
2	MC	28	19	41

The rapid decay rates calculated from the k_d values shown in Figure 2.3 indicate that the decay of $[H_2^{18}O_2]$ in the sample lines (i.e. during the 4 min travel time from mesocosm to sample syringe) should be considered. Because the conditions in the dark Norprene tubing are best represented by those in the closed-bottom control (i.e. no sediment-water interface), the k_d values

for MC can be used to estimate the significance of the sample line decay. Using the average k_d of 2.3 h^{-1} , we calculate that approximately 15% of the $\text{H}_2^{18}\text{O}_2$ could decay in 4 min. Since the $[\text{H}_2^{18}\text{O}_2]$ values, and the resulting modeled k_d values, were not corrected for the 4 min travel time, the reported k_d values might slightly over-estimate the decay rates in the mesocosms. However, whereas the H_2O_2 in MC was subjected to biotic films on the container walls, it was verified that the sample lines were free of biotic build-up (checked visually after the experimental days and evidenced by constant flow rates). This implies that the decay rates in the sample lines were likely less than that observed in MC. Further, a 15% uncertainty introduced by the sample line decay is small compared to the reported $[\text{H}_2^{18}\text{O}_2]$ uncertainty presented in Figure 2.3 (i.e. average uncertainty of $\pm 30\%$). Likewise, the possibility of a decrease in $[\text{H}_2^{18}\text{O}_2]_{\text{in}}$ over time creates negligible uncertainty in comparison to that presented in Figure 2.3, since repeating the modeling with a linear 10% decrease in $[\text{H}_2^{18}\text{O}_2]_{\text{in}}$ over approximately 8 h yielded modeled k_d values less than 10% lower than those calculated assuming constant $[\text{H}_2^{18}\text{O}_2]_{\text{in}}$.

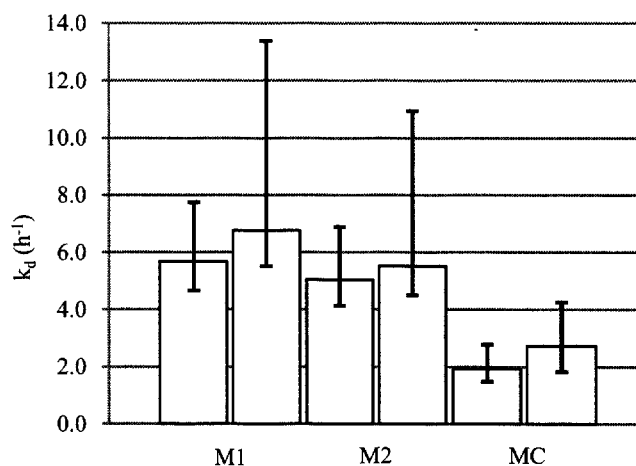


Figure 2.3. Modeled absolute decay constants (k_d) in each mesocosm. Error bars represent the k_d values associated with the 90% confidence interval upper and lower $[\text{H}_2^{18}\text{O}_2]$ listed in Table 2.2.

2.4.4 Overview of Production Processes

It is instructive to begin this discussion by qualitatively exploring the magnitude of H_2O_2 production required to yield the observed concentrations in view of the rapid rates of decay determined from the $[\text{H}_2^{18}\text{O}_2]$ data. The consistently low measured $[\text{H}_2^{18}\text{O}_2]$ values indicate H_2O_2 half-lives less than 15 min in the opened-bottom mesocosms and less than 30 min in the closed-bottom controls. Because $[\text{H}_2\text{O}_2]_{\text{in}}$ was primarily $\text{H}_2^{18}\text{O}_2$, fast production must have occurred to account for the high, increasing $[\text{H}_2\text{O}_2]$ during the light period. Further, since $[\text{H}_2\text{O}_2]$ values during the dark period indicate an apparent half-life greater than 1 h in all mesocosms, production must have continued in the dark. Based on this qualitative examination, the marked differences between $[\text{H}_2\text{O}_2]$ and $[\text{H}_2^{18}\text{O}_2]$ suggest production during both the light and dark periods. Further, the data indicate faster rates of decay, and thus production, in the opened-bottom mesocosms, suggesting that the stream bed plays a role in controlling H_2O_2 cycling in Maple Creek.

2.4.5 Modeling the Dark Production

As mentioned in section 2.4.4, dark production (P_{dark}) in Maple Creek is evidenced by the notably greater half-life of H_2O_2 with respect to $\text{H}_2^{18}\text{O}_2$. The significance of P_{dark} with respect to total H_2O_2 concentrations is illustrated by modeling $[\text{H}_2\text{O}_2]$ with the absolute decay coefficient (k_d) but neglecting the production term (i.e. (2.6) without P_{dark}). Figure 2.4 illustrates the results of this approach applied to M1 during day 1 (dotted line). As shown, measured $[\text{H}_2\text{O}_2]$ is underestimated at all time points, reaching a low steady-state within the first hour of the dark period (i.e. analogous to the $[\text{H}_2^{18}\text{O}_2]$ data).

Clearly, dark production of H_2O_2 is a significant process in Maple Creek. To investigate the behavior of this process, we explored two modeling approaches: constant P_{dark} , or time-varying P_{dark} as defined in (2.5). In the first approach, the best-fit constant P_{dark} value for each mesocosm was determined with (2.6). The results of the constant- P_{dark} model applied to M1 during day 1 are provided in Figure 2.4 (dashed line). This model also predicts a rapidly

approached steady-state $[H_2O_2]$, and consistently under-predicts measured $[H_2O_2]$ at early times and over-predicts them at late times. However, when P_{dark} is modeled as exponentially decreasing with time in the dark according to (2.5), model fits to measured $[H_2O_2]$ are very good (solid line in Figure 2.4). Modeled in this manner, P_{dark} in M1 and M2 is greater than $2 \mu\text{M h}^{-1}$ at the beginning of the dark period and decreases to near $0.5 \mu\text{M h}^{-1}$ after 3.5 h in the dark (Figure 2.5). In contrast, P_{dark} in MC are initially near $1 \mu\text{M h}^{-1}$ and decreases to less than $0.3 \mu\text{M h}^{-1}$ after 3.5 h in the dark. Dark production rates in the four opened-bottom mesocosms observed over two days are consistent with each other, and are greater than those in the closed-bottom control. As mentioned in section 2.1, the observed dark production may be comprised of both biological and abiotic (i.e. reduced metal oxidation) processes. This is discussed in section 2.5.2.

The uncertainty in P_{dark} is dependent on the uncertainty in k_d (see Figure 2.3). To bracket this uncertainty, the Microsoft Excel Solver function was utilized to determine A and b parameters that resulted in best fits of the $[H_2O_2]$ data using the 90% confidence interval high and low k_d values shown in Figure 2.3. In the four M1 and M2 experiments, the resulting high and low P_{dark} values were, on average, 21% percent lower and 43% higher, respectively, than the P_{dark} values associated with the best-fit k_d values. These average low P_{dark} values for M1 and M2 are plotted as the solid line in Figure 2.5 (the high limit is not shown since most of it is off scale). For the two MC experiments, this analysis yielded average relative uncertainties of -40% to +65%, plotted as the dashed lines in Figure 2.5. Because of the day to day differences in MC, the high P_{dark} uncertainty is based on the higher day 1 values, and the low P_{dark} uncertainty is based on the lower day 2 values.

These results indicate that, to account for the relatively slow decay of $[H_2O_2]$ in the presence of fast absolute decay rates, significant dark production must occur in the shallow freshwater system investigated. These processes would have been entirely masked had only total $[H_2O_2]$ been measured. A simple first-order decay model (i.e. analogous to (2.3) but with $[H_2O_2]$ terms replacing $[H_2^{18}O_2]$ terms) can be used to model the net changes in $[H_2O_2]$ during the dark

period. With this approach, measured $[H_2O_2]$ in all mesocosms are reasonably approximated by net k_d values of $0.4 - 0.8 h^{-1}$. This result highlights how readily dark production and the effects of the sediment-water interface (i.e. increased decay and production) are confounded by measuring only net changes in $[H_2O_2]$.

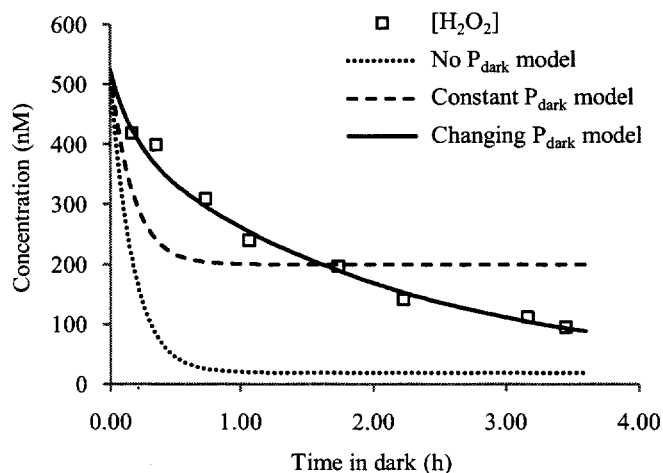


Figure 2.4. Comparison of measured and modeled $[H_2O_2]$ without P_{dark} , assuming constant P_{dark} , and changing P_{dark} according to (2.5) and (2.7).

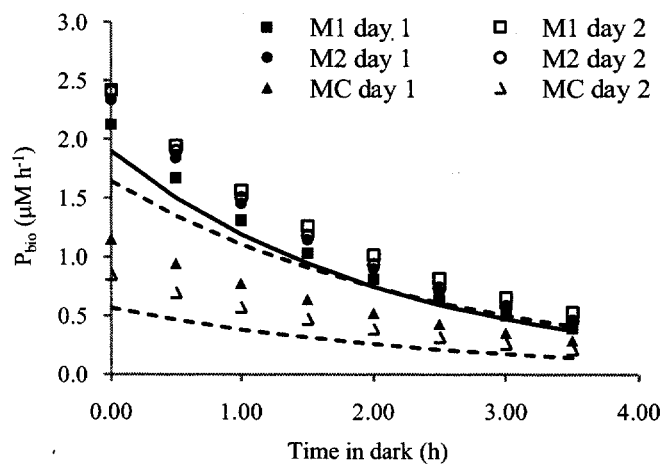
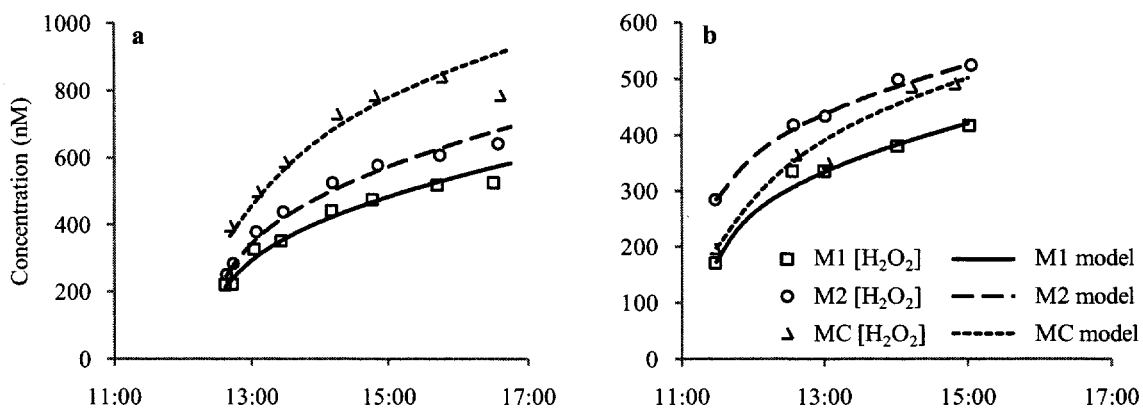


Figure 2.5. Modeled P_{dark} for each mesocosm according to (2.5) and (2.7). The uncertainty is depicted by the solid and dashed lines for the opened- and closed-bottom mesocosms, respectively. The high limit of uncertainty for M1 and M2 is not shown for scale clarity.

2.4.6 Modeling the Light Production

Evidenced by increasing $[H_2O_2]$ after the mesocosm were uncovered, light accelerates H_2O_2 production in Maple Creek. Initial attempts at modeling measured $[H_2O_2]$ assumed that the rate of H_2O_2 production during the light period (P_{light}) was constant with time according to (2.10). However, similar to the results obtained from modeling the dark period $[H_2O_2]$, this approach yields poor fits to measured $[H_2O_2]$ – i.e. a rapidly approached steady-state $[H_2O_2]$ much less than measured $[H_2O_2]$. Since H_2O_2 continues to increase instead of reaching a steady-state, this discrepancy cannot be due to changing irradiance, which mostly decreased over the course of each day (Figures 2.2a and b). Measured $[H_2O_2]$ was subsequently modeled with P_{light} increasing with time in the light according to a power law provided in section 2.3.3 (see equations (2.9) and (2.11)). The results of using the nonlinear- P_{light} model for all mesocosms are provided in Figures 2.6a and b. The slight over-predictions of the model for day 1 are probably attributable to the sharp decrease in sunlight intensity after 14:45 from mesocosm shading (see Figure 2.2a).

Using the nonlinear P_{light} model, calculated rates of total light production in M1 and M2 are $1.0 - 1.6 \mu M h^{-1}$ at the beginning of the light period and increase to $3.0 \mu M h^{-1}$ after 4 h in the light; production rates in MC are initially $0.5 - 0.8 \mu M h^{-1}$ and increase to near $1.5 \mu M h^{-1}$ after 4 h in the light (Figure 2.7). Similar to the modeled P_{dark} , P_{light} in the closed-bottom control is consistently less than that modeled in the opened-bottom mesocosms at all time points. The relative uncertainty is assumed to be equivalent to that determined for the P_{dark} values (see section 2.4.5), and is illustrated in Figure 2.7 by the solid and dashed lines for the opened- and closed-bottom mesocosms, respectively. The low limit of uncertainty for the opened-bottom mesocosms was calculated from the average associated P_{light} values at each time point (the high limit of uncertainty for M1 and M2 is not shown). Again, due to the day to day differences in MC, the high P_{light} uncertainty is based on the higher day 1 values, and the low P_{light} uncertainty is based on the lower day 2 values.



Figures 2.6a and b. Comparison of measured and modeled $[H_2O_2]$ during the light period using the nonlinear- P_{light} model (days 1 and 2 presented in a and b, respectively).

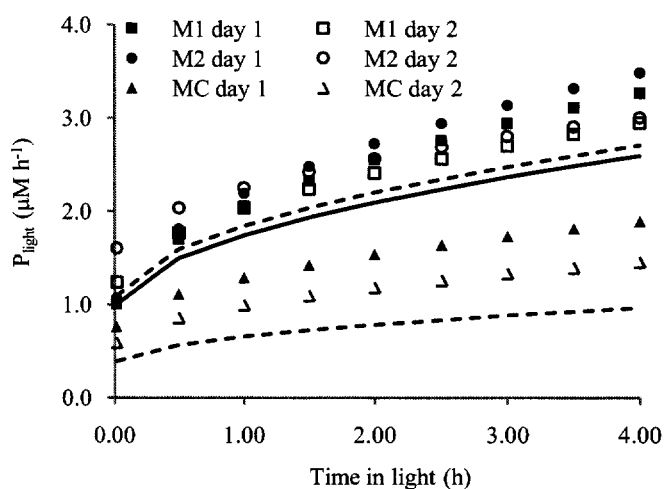


Figure 2.7. Modeled P_{light} for each mesocosm according to (2.9) and (2.11). The uncertainty is depicted by the solid and dashed lines for the opened- and closed-bottom mesocosms, respectively. The high limit of uncertainty for M1 and M2 is not shown for scale clarity.

The P_{light} term includes both abiotic photo-production (P_{photo}) and biological photo-production ($P_{bio,light}$). To characterize $P_{bio,light}$ during the light period, the contributions of P_{photo} are subtracted from P_{light} . P_{photo} in Maple Creek has previously been measured in $0.2 \mu m$ filtered surface water during the summers of 2006 and 2009, and was observed to be $0.2 - 1.0 \mu M h^{-1}$ (see section A.2). If we assume approximately $0.5 \mu M h^{-1}$ as a representative value for P_{photo} (see section A.2), $P_{bio,light}$ during day 2 increases from approximately $0.9 \mu M h^{-1}$ to approximately $2.4 \mu M h^{-1}$ at the end of light period in the opened-bottom mesocosms, and from less than $0.1 \mu M h^{-1}$

to less than $0.9 \mu\text{M h}^{-1}$ at the end of the light period in the closed-bottom control. Modeling biological photo-production in this manner is supported by the correspondence between $P_{\text{bio,light}}$ and P_{dark} at the time of transition between light and dark periods (i.e. 15:00 during day 2), since P_{photo} ceases in the absence of light. Table 2.3 lists the modeled $P_{\text{bio,light}}$ and P_{dark} values for each mesocosm during day 2 at the end of the light period and beginning of the dark period, respectively. As shown, the correspondence between these production rates is excellent, implying that P_{dark} is primarily biological dark production ($P_{\text{bio,dark}}$). This implication is discussed in greater detail in section 2.5.2.

Due to the onset of mesocosm shading (see Figure 2.2a), analogous calculations aimed at separating day 1 P_{light} into P_{photo} and $P_{\text{bio,light}}$ were not performed. However, given the overall consistencies in measured and modeled data between days 1 and 2, P_{photo} and $P_{\text{bio,light}}$ during day 1 are assumed to be similar to those reported for day 2.

Table 2.3. Agreement of $P_{\text{bio,light}}$ and P_{dark} during day 2 at the time of transition between light and dark periods (i.e. 15:00) when $P_{\text{bio,light}}$ is modeled as the difference between P_{light} and $P_{\text{photo}} = 0.5 \mu\text{M h}^{-1}$.

Mesocosm	$P_{\text{bio,light}} (\mu\text{M h}^{-1})$	$P_{\text{dark}} (\mu\text{M h}^{-1})$
M1	2.4	2.4
M2	2.4	2.4
MC	0.9	0.9

Results from modeling the light period suggest that the conventional approach of attributing all H_2O_2 production in the light to photo-oxidation of CDOM (i.e. abiotic photo-production) may greatly underestimate the cycling of H_2O_2 in freshwater systems. A simple comparison illustrates this. Referring to (2.10) but using a net k_d of 0.8 h^{-1} (discussed in section 2.4.5), the light period $[\text{H}_2\text{O}_2]$ for M1 on day 1 can be reasonably approximated with a time-changing P_{light} between $0.2 - 0.5 \mu\text{M h}^{-1}$, rates that are readily attributed to abiotic photo-production alone. Similar results were obtained by modeling all mesocosms in this manner.

Thus, analogous to modeling the dark period according to net changes in $[H_2O_2]$, total light production and the effects of the sediment-water interface (i.e. apparent increased decay and production) are masked when the light period is modeled according to net changes in $[H_2O_2]$ assuming light production is solely abiotic.

2.5 Discussion

In this section, the absolute rates of decay and production are examined with respect to their controlling mechanisms (i.e. abiotic vs. biological). We provide supporting evidence that the *in situ* rates of decay may be enhanced (vs. the closed-bottom control) via the combined effects of biofilms and mineral surfaces present at the sediment-water interface. In discussing potential sources of production, we highlight how abiotic mechanisms alone cannot account for the observed rates, both in the dark and the light, and provide supporting evidence that aquatic microbiota are the dominant sources of H_2O_2 production in Maple Creek.

2.5.1 Rates of Decay

Because this study is the first to report absolute k_d values using *in situ* measurements, direct comparisons to other studies are not possible. However, the average k_d of 2.3 h^{-1} in the closed-bottom control reasonably agrees with the $0.3 - 1.7 \text{ h}^{-1}$ range observed by Vermilyea et al. (in press) in dark incubations of unfiltered lake waters (where k_{loss, H_2O_2} is equivalent to k_d in this study). This agreement is reasonable given the absence of a sediment-water interface in both cases, and provides credibility for the methods used to measure *in situ* absolute k_d values.

The design of the mesocosm experiments aimed to distinguish any effects of the sediment-water interface, such as those induced by biofilms, from those occurring in the stream water (i.e. in the closed-bottom control). This design, which is the first of its kind, was applied in hopes of discovering a clear difference between H_2O_2 dynamics *in situ* from those occurring in conditions representative of typical incubation studies. To our knowledge, only one other study

has investigated the impacts of biofilm activity on freshwater H_2O_2 cycling. Richard et al. (2007) determined that net decay rates increased three-fold (i.e. 0.1 to 0.3 h^{-1}) in unfiltered incubations of Water of Leath, a freshwater stream in New Zealand, exposed to biotic (i.e. diatom) films. Additionally, by examining net decay rates in freshwater lake incubations passed through various filter sizes, Cooper and Lean (1989) and Cooper et al. (1994) determined that H_2O_2 decay rates were primarily controlled by small algae (i.e. < 5 μm in diameter) and bacteria, which are common biofilm constituents (O'Toole and Ghannoum 2005). Thus, the higher decay rates observed in the opened-bottom mesocosms, with respect to MC and the results reported by Vermilyea et al. (in press), suggest that biofilms present on the sediment-water interface may play a role in dictating rates of H_2O_2 decay in Maple Creek.

Although previous studies have attributed the fast rates of decay in freshwaters to biological processes (Cooper and Zepp 1990, Cooper et al. 1994), in the presence of Fe(II), abiotic mechanisms may also be important contributors. According to Emmenegger et al. (1998), the consumption of H_2O_2 via Fe(II) (i.e. the Fenton reaction) is governed by a second-order rate constant (k_{Fen}) of $10^{6.7} \text{ M}^{-1} \text{ min}^{-1}$ (or $0.3 \text{ nM}^{-1} \text{ h}^{-1}$) in pH 8.5 natural waters. Using this value of k_{Fen} , which represents an upper limit for the pH conditions in Maple Creek (see section 2.2.4), the minimum concentration of Fe(II) required to account for the decay of $\text{H}_2^{18}\text{O}_2$, calculated by equating the rate of decay (i.e. $-k_d[\text{H}_2^{18}\text{O}_2]$) to the rate of the Fenton reaction (i.e. $-k_{\text{Fen}}[\text{Fe(II)}][\text{H}_2^{18}\text{O}_2]$), is approximately 20 nM in the opened-bottom mesocosms (i.e. average $k_d = 5.7 \text{ h}^{-1}$), and less than 8 nM in the closed-bottom control (i.e. average $k_d = 2.3 \text{ h}^{-1}$). Measurements of [Fe(II)] in Maple Creek during a previous field campaign (July 2009), made by Dr. Andrew Vermilyea (University of Alaska) according to the colorimetric FIA method detailed by Pullin and Cabaniss (2001), determined that [Fe(II)] was generally less than the detection limit of 10 nM (data not shown). However, because k_{Fen} is matrix dependent and the exact value is not known for our systems, and because [Fe(II)] was not measured during the same field campaign as k_d , abiotic decay of H_2O_2 cannot be excluded as a significant control on the cycling of H_2O_2 in Maple

Creek. Further, as mentioned in section 2.1, mineral surfaces present at the sediment-water interface may account for the enhanced decay rates in the opened-bottom mesocosms with respect to the closed-bottom controls.

As mentioned in section 2.4.3, possible temporal trends in $[H_2^{18}O_2]$ were neglected in this study because they were of similar magnitude to the scatter in the data. However, we investigated the implications associated with assuming non-constant k_d values, and can illustrate the inadequacy of this approach by qualitatively exploring the differential equations describing $[H_2O_2]$ in the dark and the light. As shown in Figures 2.2a and b, $\frac{d[H_2O_2]}{dt}$ becomes less negative with time in the dark. In this study, we assumed constant k_d and exponentially decreasing P_{dark} to explain this behavior. However, an alternative explanation is decreasing k_d with time in the dark. Because it only adds complication to assume both k_d and P_{dark} are non-constant, we can alternatively assume constant P_{dark} and time-changing k_d (k_d'). Referencing (2.4), because $[H_2O_2]$ decreases and $\frac{d[H_2O_2]}{dt}$ becomes less negative with time in the dark, and with constant k_f , $[H_2O_2]_{in}$, and P_{dark} , k_d' must increase with time in the dark to model the observed $\frac{d[H_2O_2]}{dt}$. However, this would imply a decrease in $[H_2^{18}O_2]$ with time in the dark, and as shown in Figures 2.2c and d, however, measured $[H_2^{18}O_2]$ does not exhibit this trend. Similarly, we can illustrate that the observed nonlinear behavior of $\frac{d[H_2O_2]}{dt}$ during the light period is not indicative of constant P_{light} and time-changing k_d' . Referencing (2.8), because $[H_2O_2]$ increases and $\frac{d[H_2O_2]}{dt}$ decreases with time in the light (see Figures 2.2a and b), and with constant k_f , $[H_2O_2]_{in}$, and P_{light} , k_d' must decrease with time in the light to model the observed $\frac{d[H_2O_2]}{dt}$. However, measured $[H_2^{18}O_2]$ does not suggest this trend (i.e. consistently low $[H_2^{18}O_2]$ in the light, see Figures 2.2c and d). Thus, our data do not support the assumption of constant production and time-changing k_d' . However, the possibility of both k_d and production being non-constant cannot be excluded.

2.5.2 Production Processes

The results of this study strongly evidence *in situ* dark biological production occurring at rates significant to the natural H_2O_2 budget in Maple Creek. We have not characterized the modeled dark production rates (P_{dark}) as chiefly biological processes, however, without considering the potential abiotic mechanisms contributing to dark H_2O_2 production. Dark abiotic production of H_2O_2 can occur via reduction of Fe(III) and subsequent oxidation of Fe(II) by O_2 (Voelker et al. 1997, Pullin and Cabaniss 2003). As mentioned in section 2.1, Fe(II) is produced in natural waters via thermal reduction of Fe(III). Pullin and Cabaniss (2003) observed thermal reduction of Fe(III) oxyhydroxides (initially $10 \mu\text{M}$) at rates of $48 - 290 \text{ nM h}^{-1}$ in pH 8.0 waters containing 10 mg L^{-1} natural organic matter (NOM), suggesting that Fe(II) may be readily supplied via this mechanism in freshwater systems. Although [Fe(II)] is assumed to be fairly low in the Maple Creek experiments (see section 2.5.1), using equation 13 and information from Table 2 and Figure 6 in King and Farlow (2000), the formation rate of H_2O_2 due to the oxidation of a continuous supply of 10 nM Fe(II) is approximately 100 nM h^{-1} at pH 8, assuming 2 mM carbonate and 25°C (conditions representative of Maple Creek). Again, because [Fe(II)] was not measured during the August 2009 field experiments, abiotic dark production of H_2O_2 may be non-negligible to the dark cycling of H_2O_2 in Maple Creek, namely during late night and early morning. However, the modeled rates of dark production in the opened-bottom mesocosms are much greater than can be attributed to Fe(II) oxidation (see Figure 2.5). Thus, given the visible abundance of algal communities on the sediment-water interface, and variety of biochemical reactions capable of producing H_2O_2 , biological processes are evidenced as the dominant *in situ* dark production mechanisms in Maple Creek. Based on these results, we equate P_{dark} in the opened-bottom mesocosms to $P_{\text{bio,dark}}$ in the following discussion.

Because dark biological production ($P_{\text{bio,dark}}$) has only been identified in a limited number of freshwater studies (Cooper and Lean 1989, Richard et al. 2007, Vermilyea et al. in press), and its *in situ* temporal character has not previously been investigated, modeling $P_{\text{bio,dark}}$ as nonlinear

in the Maple Creek mesocosms is a new approach (see figure 2.5). In a recent freshwater incubation study, Vermilyea et al. (in press) modeled absolute dark biological rates (where $P_{H_2O_2}$ is equivalent to $P_{bio,dark}$ in this study) as remaining constant over several hours. However, in contrast to the Maple Creek mesocosms, Vermilyea's samples were not exposed to sunlight immediately prior to the incubations (i.e. samples collected before dawn). Thus, the nonlinear behavior of $P_{bio,dark}$ may only be visible upon switching suddenly from full sunlight to complete darkness, and may represent a gradual transition in cellular ROS production and enzymatic activity.

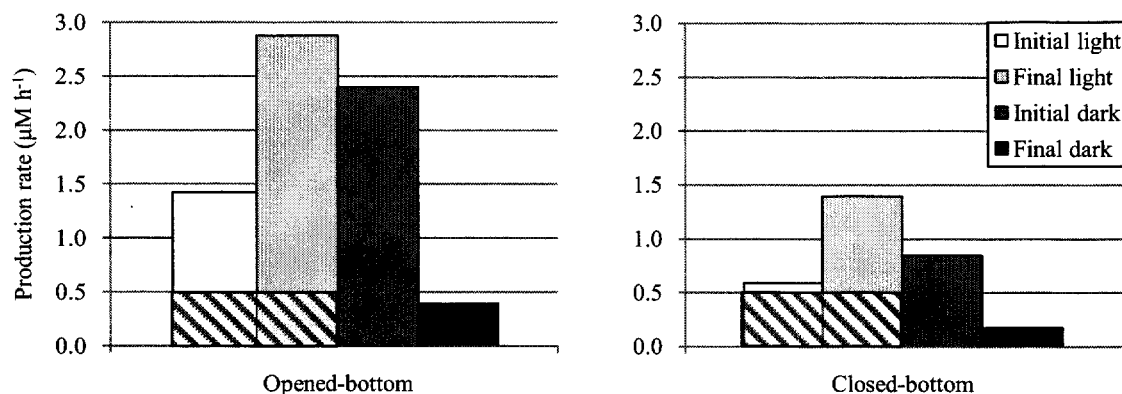
Because the cell membrane permeability of H_2O_2 is similar to water (Buettner et al. 2009), a concentration gradient can drive H_2O_2 into the exogenous medium when intracellular $[H_2O_2]$ is greater than extracellular $[H_2O_2]$ (Shtamm et al. 1991). Under high irradiance, aquatic aerobes can produce ROS at rates of $10^{-6} M s^{-1}$ during photosynthetic processes (Asada 1994), and respiration may be similarly significant in terms of ROS production (Maxwell et al. 1999). In the dark, production of ROS via the photosynthetic apparatus ceases, but respiration continues (Badger et al. 2000, Luz et al. 2002). Because ROS production via respiration is dependent on dissolved oxygen (DO) (Fridovich 1986b, Turrens 1996), the rate of ROS production might slow with time in the dark as DO is consumed. Additionally, intracellular ROS-scavenging enzymatic activity has been observed to change over the course of hours in cultures of the microalgae *Tetraselmis gracilis* exposed to high light-complete dark cycles (Sigaud-Kutner et al. 2005). Thus, a transition in intracellular ROS production and scavenging activity upon suddenly switching from the light to dark periods may account, to some extent, for the modeled nonlinear behavior of $P_{bio,dark}$ in Maple Creek. Additionally, extracellular enzymatic reactions, which are dependent on the availability of various substrates including iron, may also contribute to the nonlinear biological production of H_2O_2 in the dark (Palenik et al 1987, Twiner 2000).

As mentioned in section 2.1, biological production of H_2O_2 has been observed in the light in cultures of various aquatic microorganisms (Patterson and Myers 1973, Roncel et al. 1989,

Park et al. 1991, Zepp et al. 1992); however, the study reported here is the first to observe biological photo-production ($P_{\text{bio,light}}$) *in situ*. A key observation of the modeled $P_{\text{bio,light}}$ is that it consistently increases with time in the light (see figure 2.7, where $P_{\text{bio,light}}$ is estimated as $P_{\text{light}} - 0.5 \mu\text{M h}^{-1}$ at all time points), perhaps suggesting a positive correlation between the growth of microbiological communities inside the mesocosms and $P_{\text{bio,light}}$. This is supported by the results of Zepp et al. (1992), where photo-production of H_2O_2 was observed to increase with increasing cell density in cultures of the freshwater green algae *Chlamydomonas sp.* However, the authors also observed the ability of *Chlamydomonas sp.* to degrade H_2O_2 decreased after exposure to 5 h of sunlight, suggesting that a time-increasing $P_{\text{bio,light}}$ could also be related to photo-induced damage on ROS scavenging enzymes. Another observation of $P_{\text{bio,light}}$, as well as rates of total light production (P_{light}), is that production is modeled as leveling off near the end of the light period. This may simply be explained by the decrease in sunlight intensity, shown in Figures 2.2a and b, which is expected to impact both biological and abiotic photo-production.

The absolute, *in situ* rates of biological production reported here are the first to be documented. Previous to this study, biological photo-production has only been observed in culture studies, and its contributions to freshwater H_2O_2 cycling were entirely unknown. The results reported indicate *in situ* rates of biological photo-production approaching $3 \mu\text{M h}^{-1}$ under mid-day irradiance – rates at least several-fold greater than rates of abiotic photo-production. Additionally, we observed rapid *in situ* rates of dark production, and provided evidence for biological processes being the dominant dark production mechanisms. To signify the impact of the proposed biological production rates on the H_2O_2 budget in Maple Creek, we can integrate P_{light} , $P_{\text{bio,dark}}$ (assumed equivalent to P_{dark}), and P_{photo} with respect to time. Refer to Figures 2.8a and b for visual summaries of the calculations that follow. During the light period of day 2 (approximately 3.5 h), for the opened-bottom mesocosms we estimate that a total of $1.9 \times 10^2 \mu\text{mol H}_2\text{O}_2$ were produced, and just $4.2 \times 10^1 \mu\text{mol}$ of this were produced abiotically. Repeating these calculations for the closed-bottom control during day 2, we estimate that a total of 9.0×10^1

μmol were produced, and $4.2 \times 10^1 \mu\text{mol}$ of this were produced abiotically. Accounting for the dark period, the total amount of H_2O_2 produced *biologically* during the experimental day is estimated to be 2.7×10^2 and $9.3 \times 10^1 \mu\text{mol}$ in the opened- and closed-bottom mesocosms, respectively. Clearly, biological processes are evidenced as significant contributors to the H_2O_2 budget in Maple Creek, namely when compared to abiotic photo-production. Further, the amounts of H_2O_2 produced in M1 and M2 are estimated to be greater than that produced in MC, suggesting the need for *in situ* measurements to fully describe the cycling of H_2O_2 in freshwater systems.



Figures 2.8a and b. Bar graphs of initial and final P_{light} and P_{dark} for the opened- and closed-bottom mesocosms during day 2 (presented in a and b, respectively). The average production rates of M1 and M2 were used to calculate production rates in Figure 2.8a. The hatched boxes represent the contributions of abiotic photo-production (P_{photo}).

2.6 Conclusions

Simultaneous measurements of $[\text{H}_2^{18}\text{O}_2]$ and $[\text{H}_2\text{O}_2]$ indicate absolute decay and production occurring at rates much faster than would be discerned from observing the net changes in $[\text{H}_2\text{O}_2]$ alone. Additionally, both in the light and the dark, the rates of decay and production appear to be enhanced in the opened-bottom mesocosms, suggesting that processes occurring at the sediment-water interface impact the cycling of H_2O_2 in Maple Creek. These results highlight the importance of *in situ* vs. incubation measurements to fully understand the cycling of H_2O_2 in

freshwater systems. Further, in stark contrast to the conventional wisdom that H_2O_2 production in freshwaters is largely governed by abiotic photo-production, the results of this study imply that microbiological communities largely govern H_2O_2 production Maple Creek.

Future work is necessitated to understand which organisms (i.e. algae, fungi, or bacteria) are the sources of H_2O_2 production, both in the light and the dark, and which are predominantly sinks of H_2O_2 . Further, the time and/or light dependence of biological production needs further investigation, as do the biochemical mechanisms responsible for the production, in order to accurately describe freshwater H_2O_2 cycling. Additionally, given the potential importance of Fe(II) in the decay and production of H_2O_2 in Maple Creek, temporal measurements of [Fe(II)] in conjunction with [H_2O_2] and [$\text{H}_2^{18}\text{O}_2$] are required to better understand the significance of abiotic contributions to freshwater H_2O_2 budgets.

REFERENCES CITED

- Asada, Y., M. Miyabe, M. Kikkawa, and M. Kuwahara. 1986. Oxidation of NADH by a peroxidase of a lignin-degrading basidiomycete, *Phanerochaete-chrysosporium*, and its involvement in the degradation of a lignin model-compound. *Agr. Biol. Chem. Tokyo*. **50**: 525-529.
- Asada, K., and M. Takahashi. 1987. Production and scavenging of active oxygen in photosynthesis, p. 227-287. *In* D. J. Kyle, C. B. Osmond, and C. J. Arntzen [eds.], *Photoinhibition*. Elseviers.
- Asada, K. 1994. Production and action of active oxygen species in photosynthetic tissues, p. 77-104. *In* C. Foyer and P. Mullineaux [eds.], *Photooxidative Stresses in Plants: Causes and Amelioration*. CRC Press Inc.
- Badger, M. R., S. von Caemmerer, S. Ruuska, and H. Nakano. 2000. Electron flow to oxygen in higher plants and algae: rates and control of direct photoreduction (Mehler reaction) and rubisco oxygenase. *Phil. Trans. R. Soc. Lond. B*. **355**: 1433-1446.
- Bischof, K., P. L. Janknegt, A. G. J. Buma, J. W. Rijstenbil, G. Peralta, and A. M. Breeman. 2003. Oxidative stress and enzymatic scavenging of superoxide radicals induced by solar UV-B radiation in *Ulva* canopies from southern Spain. *Sci. Mar.* **67**: 353-359.
- Buettner, G. R., C. F. Ng, M. Wang, V. G. J. Rodgers, and F. Q. Schafer. 2009. A new paradigm: manganese superoxide dismutase influences the production of H₂O₂ in cells and thereby their biological state. *Free Rad. Bio. Med.* **41**: 1338-1350.
- Byegard, J., G. Skarnemark, and M. Skalberg. 1999. The stability of some metal EDTA, DTPA, and DOTA complexes: application as tracers in groundwater studies. *J. Radioanal. Nucl. Ch.* **241**: 281-290.
- Capel, P. D., K. A. McCarthy, and J. E. Barbash. 2008. National, holistic, watershed-scale approach to understand the sources, transport, and fate of agricultural chemicals. *J. Environ. Qual.* **37**: 983-993.
- Collen, J., M. J. Delrio, G. Garciareina, and M. Pedersen. 1995. Photosynthetic production of hydrogen-peroxide by *Ulva rigida* C. Ag. (Chlorophyta). *Planta*. **196**: 225-230.
- Cooper, W. J., R. G. Zika, R. G. Petasne, and J. M. C. Plane. 1988. Photochemical formation of H₂O₂ in natural waters exposed to sunlight. *Environ. Sci. Technol.* **22**: 1156-1160.
- Cooper, W. J., and D. R. S. Lean. 1989. Hydrogen peroxide concentration in a northern lake: photochemical formation and diel variability. *Environ. Sci. Technol.* **23**: 1425-1428.
- Cooper, W. J., and R. G. Zepp. 1990. Hydrogen-peroxide decay in waters with suspended soils: evidence for biologically mediated processes. *Can. J. Fish. Aquat. Sci.* **47**: 888-893.

- Cooper, W. J., C. W. Shao, D. R. S. Lean, A. S. Gordon, and F. E. Scully. 1994. Factors affecting the distribution of H₂O₂ in surface waters, p. 391-422. *In Environmental Chemistry of Lakes and Reservoirs*. Adv. Chem. Ser.
- Cooper, W. J., J. K. Moegling, R. J. Kieber, and J. J. Kiddle. 2000. A chemiluminescence method for the analysis of H₂O₂ in natural waters. *Mar. Chem.* **70**: 191-200.
- Diem, D., and W. Stumm. 1984. Is dissolved Mn²⁺ being oxidized by O₂ in absence of Mn-bacteria or surface catalysts? *Geochim. Cosmochim. Ac.* **48**: 1571-1573.
- Dingman, S. L. 2002. Basic hydrologic concepts, p. 24-25. *In Physical Hydrology*, 2nd ed. Prentice Hall.
- Draper, W. M., and D. G. Crosby. 1983. The photochemical generation of hydrogen peroxide in natural waters. *Arch. Environ. Contam. Toxicol.* **12**: 121-126.
- Emmenegger, L., D. W. King, L. Sigg, and B. Sulzberger. 1998. Oxidation kinetics of Fe(II) in a eutrophic Swiss lake. *Environ. Sci. Technol.* **32**: 2990-2996.
- Fredrick, B. S., J. I. Linard, and J. L. Carpenter. 2006. Environmental setting of Maple Creek Watershed, Nebraska. Scientific Investigations Report 2006-5037. U. S. Geological Survey.
- Fridovich, I. 1986. Biological effects of the superoxide radical. *Arch. Biochem. Biophys.* **247**: 1-11.
- Fridovich, I. 1986. Superoxide dismutases. *Adv. Enzymol. RAMB.* **58**: 61-97.
- Kaltenbach, M.S., and M.A. Arnold. 1992. Acridinium ester chemiluminescence: pH dependent hydrolysis of reagents and flow injection analysis of hydrogen peroxide and glutamate. *Mikrochim. Acta.* **108**: 205-219.
- Kersten, P. J., and T. K. Kirk. 1987. Involvement of a new enzyme, glyoxal oxidase, in extracellular H₂O₂ production by *Phanerochaete chrysosporium*. *J. Bacteriol.* **169**: 2195-2201.
- King, D. W. 1998. Role of carbonate speciation on the oxidation rate of Fe(II) in aquatic systems. *Environ. Sci. Technol.* **32**: 2997-3003.
- King, D. W., and R. Farlow. 2000. Role of carbonate speciation on the oxidation of Fe(II) by H₂O₂. *Mar. Chem.* **70**: 201-209.
- King, D. W., et al. 2007. Flow injection analysis of H₂O₂ in natural waters using acridinium ester chemiluminescence: method development and optimization using a kinetic model. *Anal. Chem.* **79**: 4169-4176.
- Kwan, W. P., and B. M. Voelker. 2003. Rates of hydroxyl radical generation and organic compound oxidation in mineral-catalyzed Fenton-like systems. *Environ. Sci. Technol.* **37**: 150-1158.

- Littig, J. S., and T. A. Nieman. 1993. Flow injection chemiluminescence study of acridinium ester stability and kinetics of decomposition. *J. Biolumin. Chemilumin.* **8**: 25-31.
- Liu, W., D. W. T. Au, D. M. Anderson, P. K. S. Lam, and R. S. S. Wu. 2007. Effects of nutrients, salinity, pH and light:dark cycle on the production of reactive oxygen species in the alga *Chattonella marina*. *J. Exp. Mar. Biol. Ecol.* **346**: 76-86.
- Luz, B., E. Barkan, and Y. Sagi. 2002. Evaluation of community respiratory mechanisms with oxygen isotopes: A case study in Lake Kinneret. *Limnol. Oceanogr.* **47**: 33-42.
- Martin, J. L., and S. C. McCutcheon. 1998. Mixing in lakes and reservoirs, p. 385-427. *In* *Hydrodynamics and Transport for Water Quality Modeling*. CRC Press.
- Maxwell, D. P., Y. Wang, and L. McIntosh. 1999. The alternative oxidase lowers mitochondrial reactive oxygen production in plant cells. *Proc. Natl. Acad. Sci. USA* **96**: 8271-8276.
- Mehler, A. H. 1951. Studies on reactions of illuminated chloroplasts. I. Mechanism of the reduction of oxygen and other Hill reagents. *Arch. Biochem.* **33**: 65-67.
- Miller W. L., and D. R. Kester. 1988. Hydrogen peroxide measurement in seawater by (para-hydroxyphenyl)acetic acid dimerization. *Anal. Chem.* **60**: 2711-2715.
- Miller, G. W., et al. 2005. Hydrogen peroxide method intercomparison study in seawater. *Mar. Chem.* **97**: 4-13.
- Moffett, J., and O. Zafiriou. 1990. An investigation of hydrogen peroxide chemistry in surface waters of Vineyard Sound with H₂18O₂ and 18O₂. *Limnol. Oceanogr.* **35**: 1221 - 1229.
- Morgan, J. J. 2005. Kinetics of reaction between O₂ and Mn(II) species in aqueous solutions. *Geochim. Cosmochim. Ac.* **69**: 35-48.
- O'Toole, G. A., and M. Ghannoum. 2004. Introduction to biofilms: conceptual themes, p. 1-3. *In* *Microbial Biofilms*. ASM Press.
- Nico, P. S., C. Anastasio, and R. J. Zasoski. 2002. Rapid photo-oxidation of Mn(II) mediated by humic substances. *Geochim. Cosmochim. Ac.* **66**: 4047-4056.
- Palenik, B., O. C. Zafiriou, and F. M. M. Morel. 1987. Hydrogen peroxide production by a marine phytoplankter. *Limnol. Oceanogr.* **32**: 1365-1369.
- Park, I. H., K. K. Rao, and D. O. Hall. 1991. Photoproduction of hydrogen, hydrogen peroxide and ammonia using immobilized cyanobacteria. *Int. J. Hydrogen Energy.* **16**: 313-318.
- Paszczynski, A., V. B. Huynh, and R. Crawford. 1986. Comparison of ligninase-I and peroxidase-M2 from the white-rot fungus *Phanerochaete chrysosporium*. *Arch. Biochem. Biophys.* **244**: 750-765.
- Patterson, C. O. P., and J. Myers. 1973. Photosynthetic production of hydrogen peroxide by *Anacystis nidulans*. *Plant Physiol.* **51**: 104-109.

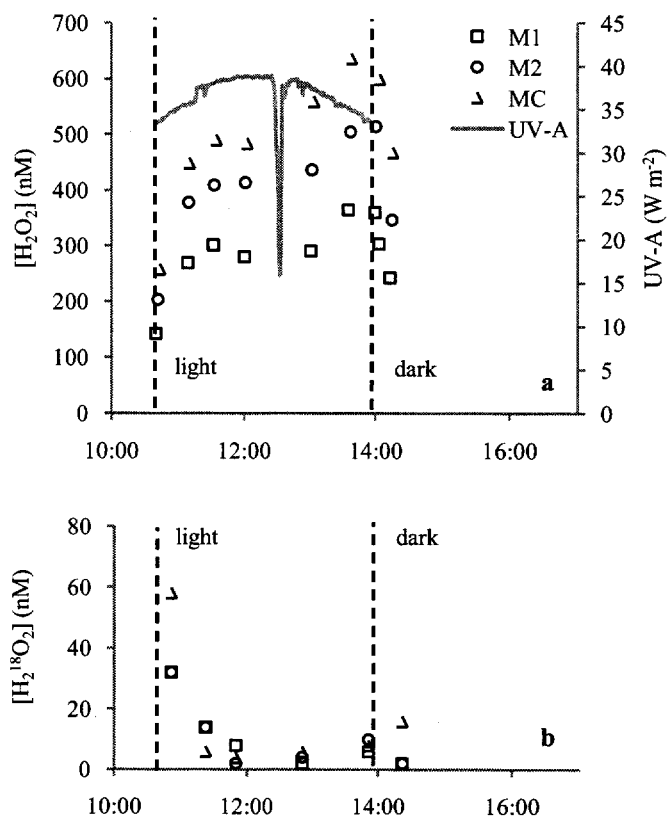
- Petigara, B. R., N. V. Blough, and A. C. Mignerey. 2002. Mechanisms of hydrogen peroxide decomposition in soils. *Environ. Sci. Technol.* **36**: 639-645.
- Puckett, L. J., et al. 2008. Transport and fate of nitrate at the ground-water/surface-water interface. *J. Environ. Qual.* **37**: 1034-1050.
- Pullin, M. J., and S. E. Cabaniss. 2001. Colorimetric flow-injection analysis of dissolved iron in high DOC waters. *Wat. Res.* **35**: 363-372.
- Pullin, M. J., and S. E. Cabaniss. 2003. The effects of pH, ionic strength, and iron-fulvic acid interactions on the kinetics of nonphotochemical iron transformations. II. The kinetics of thermal reduction. *Geochim. Cosmochim. Ac.* **67**: 4079-4089.
- Pullin, M. J., S. Bertilsson, J. V. Goldstone, and B. M. Voelker. 2004. Effects of sunlight and hydroxyl radical on dissolved organic matter: bacterial growth efficiency and production of carboxylic acids and other substrates. *Limnol. Oceanogr.* **49**: 2011-2022.
- Richard, L. E., B. M. Peake, S. A. Rusak, W. J. Cooper, and D. J. Burritt. 2007. Production and decomposition dynamics of hydrogen peroxide in freshwater. *Environ. Chem.* **4**: 49-54.
- Roncel, M., J. A. Navarro, and M. A. Delarosa. 1989. Coupling of solar energy to hydrogen peroxide production in the cyanobacterium *Anacystis nidulans*. *Appl. Environ. Microbiol.* **55**: 483-487.
- Scott, D. T., D. M. McKnight, B. M. Voelker, and D. C. Hrncir. 2002. Redox processes controlling manganese fate and transport in a mountain stream. *Environ. Sci. Technol.* **36**: 453-459.
- Shtamm, E. V., A. P. Purmal, and Y. I. Skurlatov. 1991. Role of hydrogen peroxide in natural aquatic media. *Russ. Chem. Rev.* **60**: 2373-2411.
- Sigaud-Kutner, T. C. S., A. M. P. Neto, E. Pinto, and P. Colepicolo. 2005. Diel activities of antioxidant enzymes, photosynthetic pigments and malondialdehyde content in stationary-phase cells of *Tetraselmis gracilis* (Prasinophyceae). *Aquat. Bot.* **82**: 239-249.
- Southworth, B. A., and B. M. Voelker. 2003. Hydroxyl radical production via the photo-Fenton reaction in the presence of fulvic acid. *Environ. Sci. Technol.* **37**: 1130-1136.
- Steiger, H. M., and E. Beck. 1981. Formation of hydrogen peroxide and oxygen dependence of photosynthetic CO₂ assimilation by intact chloroplasts. *Plant Cell Physiol.* **22**: 561-576.
- Stumm, W., and J. J. Morgan. 1996. *Aquatic Chemistry*, 3rd ed. Wiley.
- Sunda, W. G., S. A. Huntsman, and G. R. Harvey. 1983. Photoreduction of manganese oxides in seawater and its geochemical and biological implications. *Nature.* **301**: 234-236.
- Turrens, J. F. 1996. Superoxide production by the mitochondrial respiratory chain. *Bioscience Rep.* **17**: 3-8.

- Twiner, M. J., and C. G. Trick. 2000. Possible physiological mechanisms for production of hydrogen peroxide by the ichthyotoxic flagellate *Heterosigma akashiwo*. *J. Plankton Res.* **22**: 1961-1975.
- Vermilyea, A. W., and B. M. Voelker. 2009. Photo-Fenton reaction at near-neutral pH. *Environ. Sci. Technol.* **43**: 6927-6933.
- Vermilyea, A. W. 2009. Hydrogen peroxide in natural waters. Ph.D. thesis. Colorado School of Mines.
- Vermilyea, A. W., T. C. Dixon, and B. M. Voelker. In press. Use of $H_2^{18}O_2$ to measure absolute rates of dark H_2O_2 production in freshwater systems. *Environ. Sci. Technol.*
- Voelker, B. M., F. M. M. Morel, and B. Sulzberger. 1997. Iron redox cycling in surface waters: effects of humic substances and light. *Environ. Sci. Technol.* **34**: 1004-1011.
- Zepp, R. G., Y. I. Skurlatov, and J. T. Pierce. 1992. Algal-induced decay and formation of hydrogen peroxide in water: its possible role in oxidation of anilines by algae, p. 215-224. *In* R. G. Zika and W. J. Cooper [eds.], *Photochemistry of Environmental Aquatic Systems*, ACS Symposium Series, vol. 327. ACS.

APPENDIX

A.1. Data from 24 August 2009

A third consecutive experimental day was conducted at the Maple Creek field site during the August 2009 field campaign. All experimental conditions on the third day were equivalent to those employed on the first two days (i.e. 22 and 23 August 2009), except that no mesocosms were pH amended. The measurements of $[H_2O_2]$, $[H_2^{18}O_2]$, and UV-A collected during 24 August 2009 are provided in Figures A.1a and b. Because the data sets were not complete (i.e. absence of full dark period data), the measurements were not included in the analysis described in Chapter 2.

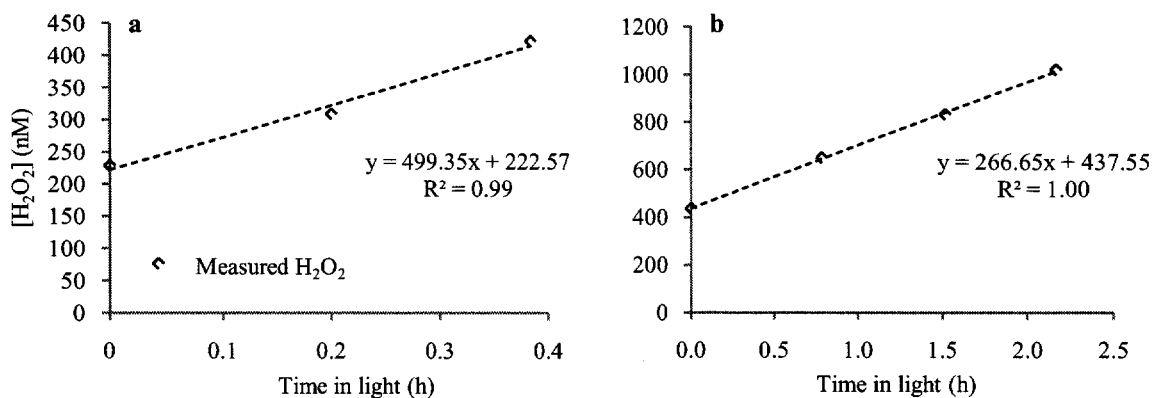


Figures A.1a and b. Measurements of $[H_2O_2]$ and $[H_2^{18}O_2]$ (a and b, respectively) during 24 August 2009. Measurements were not continued into the afternoon dark period due to power generator failure.

A.2. Direct Measurement of Abiotic Photo-Production

During previous field campaigns (summers of 2006 and 2009), we collected 0.2 μm filtered Maple Creek surface water and measured abiotic photo-production under mid-day sunlight irradiance. Figures A.2a and b present measurements of $[\text{H}_2\text{O}_2]$, in 0.2 μm filtered surface water in 125 ml quartz flasks partially submerged in Maple Creek water, on 26 July and 1 August 2009, respectively (first measurements in both experiments were collected at approximately 14:00). As shown by the slopes of the linear trendlines, the rates of abiotic photo-production (P_{photo}) on the two days were determined to be 500 and 267 nM h^{-1} (or 0.5 and 2.7 $\mu\text{M h}^{-1}$), respectively. During the summer of 2006, previous co-worker Dr. Andrew Vermilyea (University of Alaska) performed similar measurements and determined P_{photo} values near 1 $\mu\text{M h}^{-1}$ (data not shown).

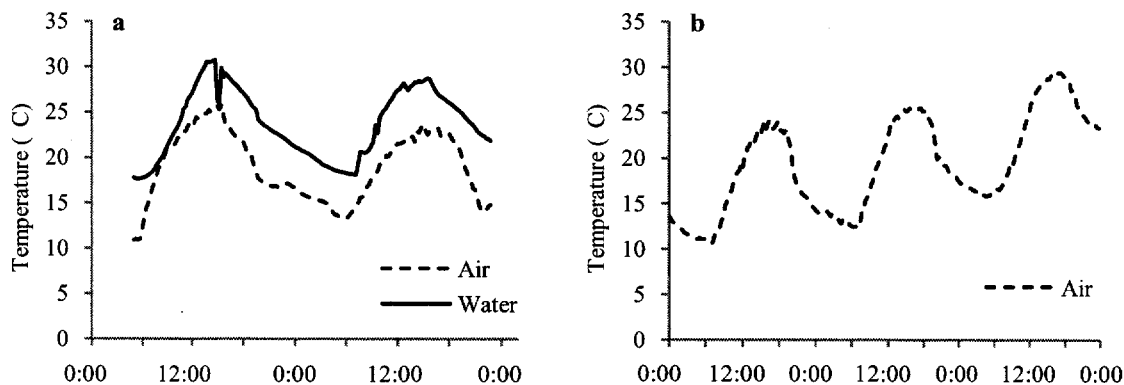
Also, during 28 – 30 July 2009 dissolved organic carbon (DOC) samples were collected from mesocosm systems equivalent to those described in Chapter 2, and revealed DOC levels in Maple Creek remained approximately constant at 3 mg L^{-1} throughout the duration of the July field campaign (DOC sample collection and analysis was performed by Dr. Durelle Scott, Virginia Polytechnic and State University). DOC samples were not analyzed during the August 2009 field campaign described in Chapter 2, and temporal variability in DOC could account for the observed range in P_{photo} (Cooper et al. 1994). Thus, in Chapter 2 we did not estimate P_{photo} at 0.5 $\mu\text{M h}^{-1}$ based on the assumed equivalence of DOC during the August 2009 trip, but based on it being a representative value within the range of P_{photo} measurements. However, the constant nature of DOC levels measured during the July 2009 campaign suggests that P_{photo} in Maple Creek can be assumed constant in the light given constant sunlight irradiance.



Figures A.2a and b. Measurements of [H₂O₂] in 0.2 μ m filtered Maple Creek surface water on 26 July and 1 August 2009 in a and b, respectively. Samples collected from 125 ml quartz flasks exposed to mid-day sunlight. The slopes of the trendlines represent the abiotic photo-production rate (units in nM h⁻¹).

A.3. Temperature Measurements

During the July 2009 field campaign to the Maple Creek field site, water temperature was measured in mesocosm systems equivalent to those described in Chapter 2 using a temperature probe (YSI). As shown in Figure A.3a, comparing the measured water temperatures with air temperatures measured on the same days (29 and 30 July 2009) at the USGS gauging station 06800000 (approximately 250 m downstream of the field site) indicates water temperatures are closely approximated by air temperatures (just an average 5°C warmer than air temperatures). In figure A.3b, we show air temperatures measured by the USGS during 22 – 24 August 2009. As shown, the air temperatures, and thus presumably the water temperatures (the YSI probe was not available for these experiments), were consistent between 22 and 23 August 2009 (i.e. days 1 and 2 in Chapter 2). Further, the temperatures only fluctuated by approximately 6°C over the course of the experiments (i.e. 11:30 – 20:30), suggesting an absence of drastic temperature effects.



Figures A.3a and b. Plot of air temperature (measured at USGS gauging station 06800000 approximately 250 m downstream of the field site) and water temperature (measured with a temperature probe at the field site) for 29 and 30 July 2009 (Figure A.3a). Plot of air temperature measured by the USGS during 22 – 24 August 2009 (Figure A.3b). As shown, the air, and presumably water, temperatures were similar on days 1 and 2.

A.4. Ratio of $^{18}\text{O}_2$ to Total Dissolved Oxygen

For the analysis presented in Chapter 2, it is important to consider the total amount of $^{18}\text{O}_2$ added to the mesocosms (i.e. in the form of $\text{H}_2^{18}\text{O}_2$) with respect to total dissolved oxygen (DO) in the mesocosm chambers. If the total amount of $^{18}\text{O}_2$ added to mesocosms is a significant fraction of DO, measurements of $\text{H}_2^{18}\text{O}_2$ in the mesocosms (i.e. through abiotic and/or biological reduction of $^{18}\text{O}_2$) might be in error – that is, measured $[\text{H}_2^{18}\text{O}_2]$ might account for the input $\text{H}_2^{18}\text{O}_2$ and $\text{H}_2^{18}\text{O}_2$ produced in the mesocosms. Using the average input rate of 82.5 ml min^{-1} and the concentration of $\text{H}_2^{18}\text{O}_2$ in the input (i.e. 400 nM), we calculate $33 \text{ nmol min}^{-1} \text{ H}_2^{18}\text{O}_2$ were added to the mesocosms (using the average mesocosm water volume of 24 L). Over the course of the approximately 8 h experimental days described in Chapter 2, this equates to a total mesocosm input of $16 \text{ } \mu\text{mol H}_2^{18}\text{O}_2$. Assuming all added $\text{H}_2^{18}\text{O}_2$ was oxidized to $^{18}\text{O}_2$ and all $^{18}\text{O}_2$ remained in the mesocosms, which likely grossly overestimates the amount of $^{18}\text{O}_2$ in the mesocosms, the total possible amount of $^{18}\text{O}_2$ added is just a fraction of DO – less than 1% (assuming DO at saturation of $250 \text{ } \mu\text{M}$). Thus, we reasonably assume that measured $[\text{H}_2^{18}\text{O}_2]$ are representative of decay processes acting only on the 400 nM added $\text{H}_2^{18}\text{O}_2$, and that $\text{H}_2^{18}\text{O}_2$ production in the mesocosms is negligible.